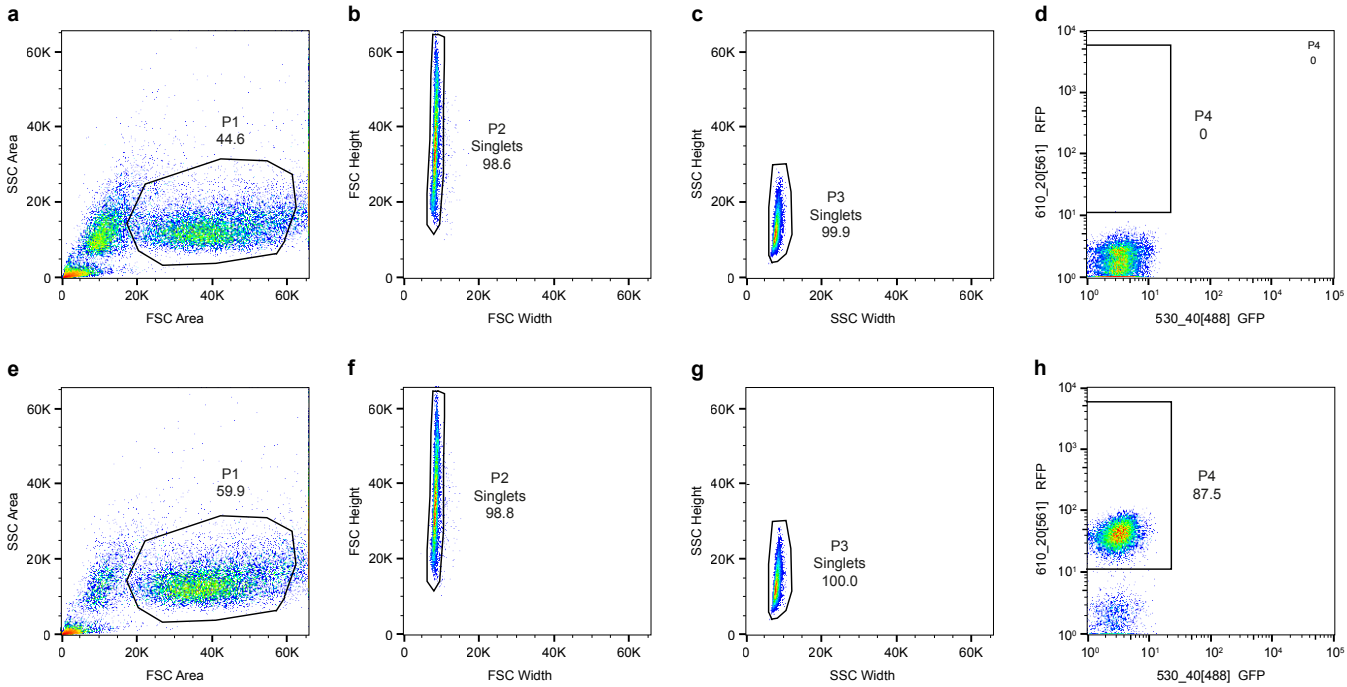
Polycomb Chromatin Topology Enables Long-Range Enhancer Recruitment during Craniofacial Development

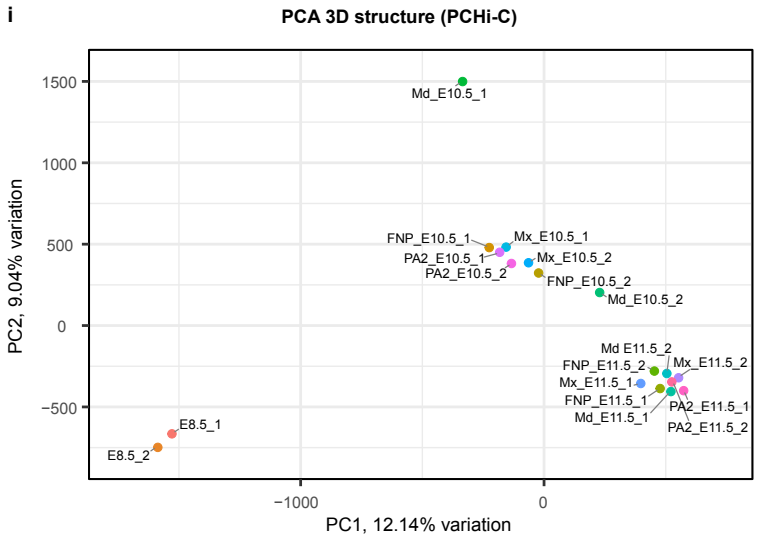
Ben Zouari et al.

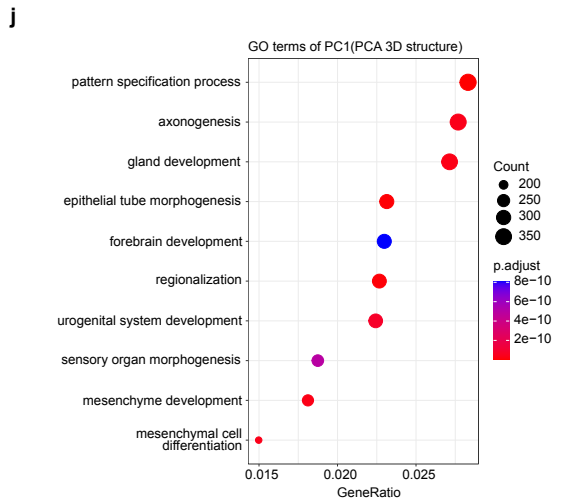
Supplementary Information

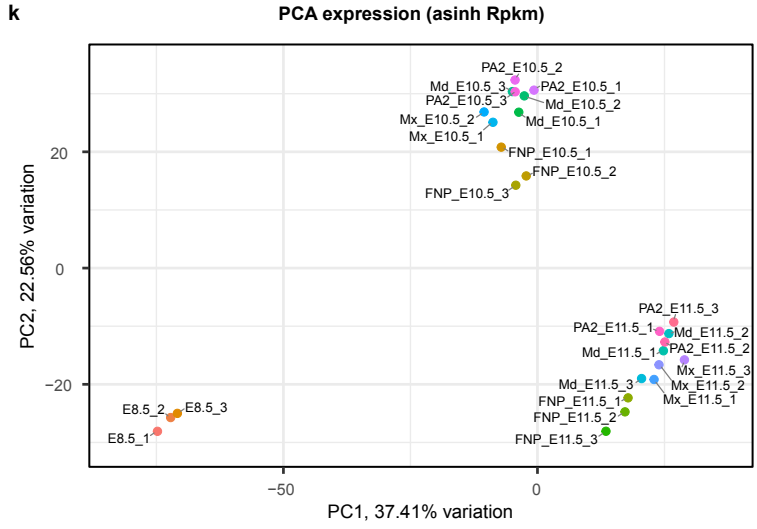
Contents:

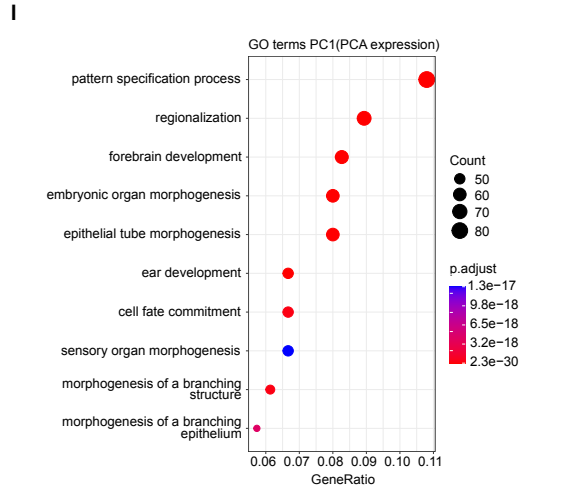
Supplementary Figs. 1 to 23
Legends of Supplementary Figs. 1 to 23


a
SSC Area
FSC Area
P1
44.6
b
FSC Height
FSC Width
P2
Singlets
98.6
c
SSC Height
SSC Width
P3
Singlets
99.9
d
610_20[561] RFP
530_40[488] GFP
P4
0
e
SSC Area
FSC Area
P1
59.9
f
FSC Height
FSC Width
P2
Singlets
98.8
g
SSC Height
SSC Width
P3
Singlets
100.0
h
610_20[561] RFP
530_40[488] GFP
P4
87.5


i
PCA 3D structure (PCHi-C)
PC2, 9.04% variation
PC1, 12.14% variation
Md_E10.5_1
FNP_E10.5_1
Mx_E10.5_1
PA2_E10.5_1
Mx_E10.5_2
PA2_E10.5_2
FNP_E10.5_2
Md_E10.5_2
Md E11.5_2
FNP_E11.5_2
Mx_E11.5_2
Mx_E11.5_1
FNP_E11.5_1
PA2_E11.5_1
Md_E11.5_1
PA2_E11.5_2
E8.5_1
E8.5_2

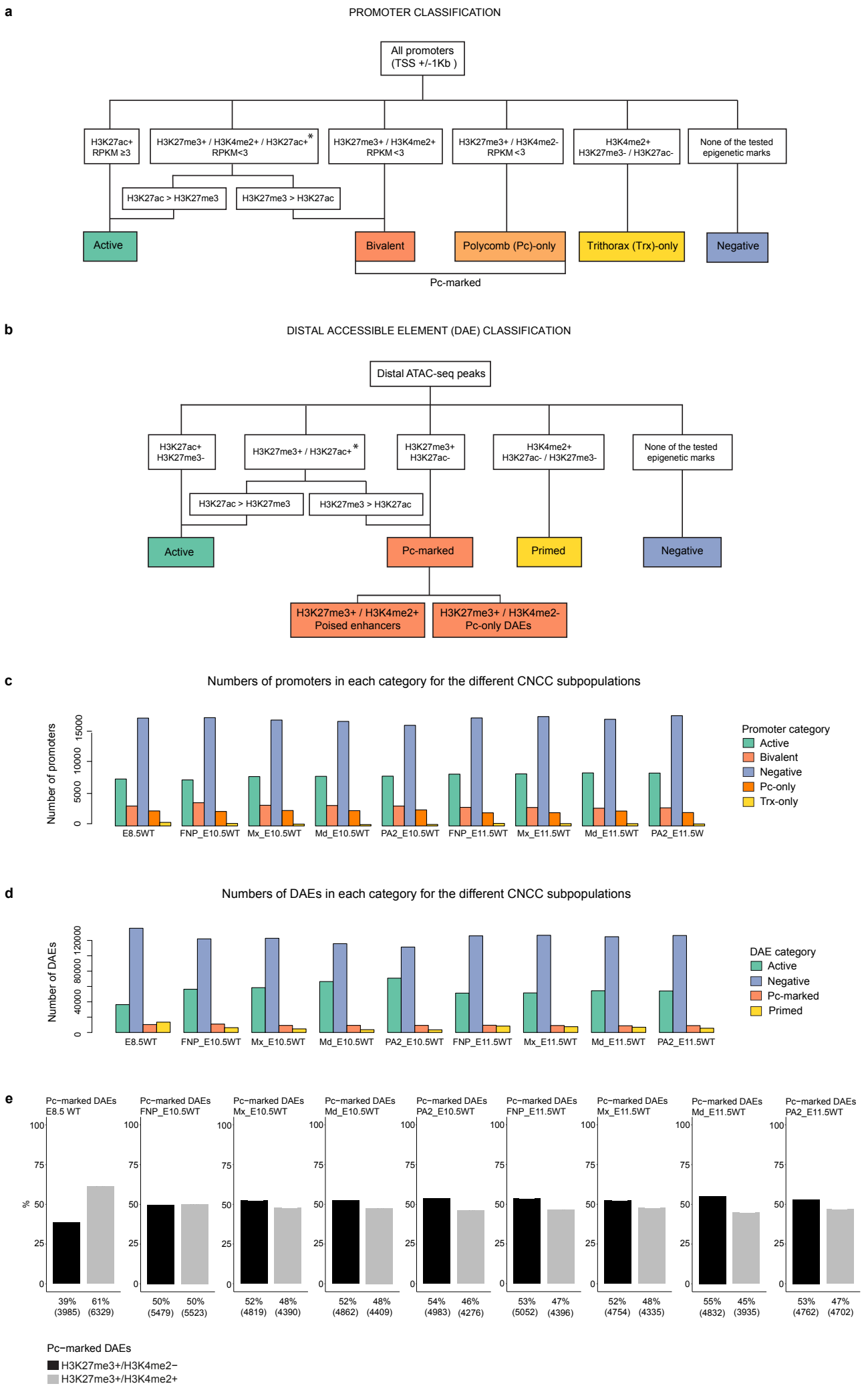

j
GO terms of PC1(PCA 3D structure)
pattern specification process
axonogenesis
gland development
epithelial tube morphogenesis
forebrain development
regionalization
urogenital system development
sensory organ morphogenesis
mesenchyme development
mesenchymal cell differentiation
GeneRatio
Count
p.adjust


k
PCA expression (asinh Rpkm)
PC2, 22.56% variation
PC1, 37.41% variation
PA2_E10.5_2
Md_E10.5_3
PA2_E10.5_1
PA2_E10.5_3
Md_E10.5_2
Mx_E10.5_2
Md_E10.5_1
Mx_E10.5_1
FNP_E10.5_1
FNP_E10.5_2
FNP_E10.5_3
PA2_E11.5_3
PA2_E11.5_1
Md_E11.5_2
Md_E11.5_1
PA2_E11.5_2
Mx_E11.5_3
Md_E11.5_3
Mx_E11.5_2
FNP_E11.5_1
Mx_E11.5_1
FNP_E11.5_2
FNP_E11.5_3
E8.5_2
E8.5_3
E8.5_1


l
GO terms PC1(PCA expression)
pattern specification process
regionalization
forebrain development
embryonic organ morphogenesis
epithelial tube morphogenesis
ear development
cell fate commitment
sensory organ morphogenesis
morphogenesis of a branching structure
morphogenesis of a branching epithelium
GeneRatio
Count
p.adjust

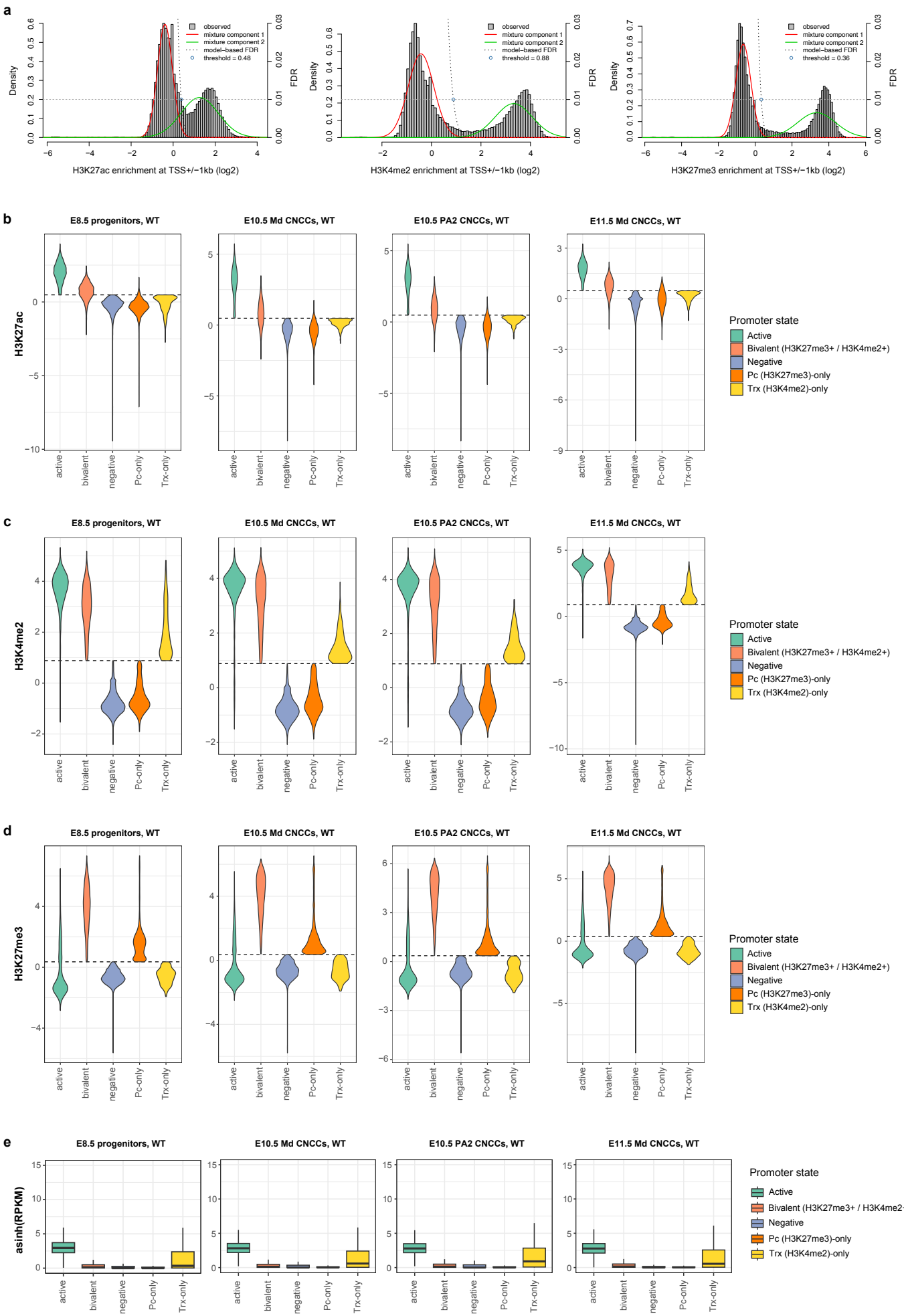
Supplementary Figure 1: FACS gating strategy and integrative analysis of PCHi-C and RNA-seq datasets from pre- and post-migratory cranial neural crest cells

(a-h) FACS of Red Fluorescent Protein (RFP)-positive cranial neural crest cells (CNCCs). Cells are first distinguished from debris based on scatter properties (P1; forward scatter (FSC)-Area versus side scatter (SSC)-Area) (**a**, **e**). Single cells are then discriminated from doublets, first using forward scatter (FSC-Width versus FSC-Height; P2) (**b**, **f**), followed by side scatter (SSC-Width versus SSC-Height; P3) (**c**, **g**). Cells are subsequently sorted based on the fluorescent marker of interest (**h**). The baseline fluorescent signal is determined using a negative control embryo from the same litter, which does not express RFP (**d**). (**i-k**) Principal component analysis (PCA) plots of Promoter-Capture Hi-C (PCHi-C) (**i**) and RNA (**k**) data from WT E8.5 pre-migratory progenitors and post-migratory CNCC subpopulations (fontonasal process, FNP; Maxillary, Mx; Mandibular, Md; and second pharyngeal arch, PA2) at E10.5 and E11.5; PCHi-C and RNA-seq assays include n=2 and n=3 biological replicates per sample, respectively. (**j-l**) Gene ontology (GO) analysis of the highest loading components from PCA analysis of PCHi-C (**i**) and RNA-seq (**k**). Significantly enriched GO terms highlight processes involved in CNCC pattern specification, confirming that these assays robustly capture structural chromatin dynamics and gene expression changes during craniofacial development.

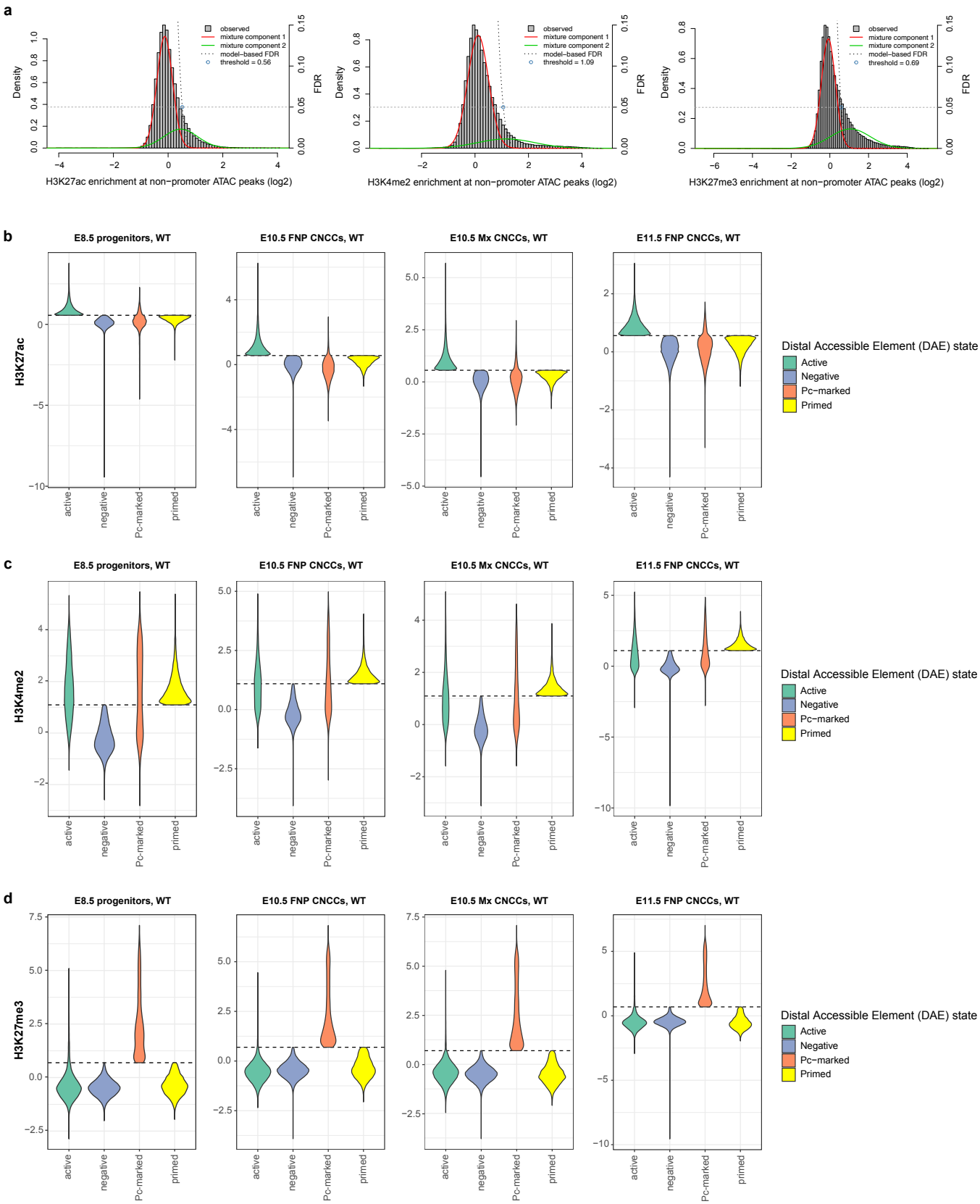

a
PROMOTER CLASSIFICATION
All promoters (TSS +/-1Kb)
H3K27ac+ RPKM ≥3
H3K27me3+ / H3K4me2+ / H3K27ac+* RPKM<3
H3K27me3+ / H3K4me2+ RPKM <3
H3K27me3+ / H3K4me2- RPKM <3
H3K4me2+ H3K27me3- / H3K27ac-
None of the tested epigenetic marks
H3K27ac > H3K27me3
H3K27me3 > H3K27ac
Active
Bivalent
Polycomb (Pc)-only
Trithorax (Trx)-only
Negative
Pc-marked
b
DISTAL ACCESSIBLE ELEMENT (DAE) CLASSIFICATION
Distal ATAC-seq peaks
H3K27ac+ H3K27me3-
H3K27me3+ / H3K27ac+*
H3K27me3+ H3K27ac-
H3K4me2+ H3K27ac- / H3K27me3-
None of the tested epigenetic marks
H3K27ac > H3K27me3
H3K27me3 > H3K27ac
Active
Pc-marked
Primed
Negative
H3K27me3+ / H3K4me2+ Poised enhancers
H3K27me3+ / H3K4me2- Pc-only DAEs
c
Numbers of promoters in each category for the different CNCC subpopulations
Number of promoters
0
5000
10000
15000
E8.5WT
FNP_E10.5WT
Mx_E10.5WT
Md_E10.5WT
PA2_E10.5WT
FNP_E11.5WT
Mx_E11.5WT
Md_E11.5WT
PA2_E11.5W
Promoter category
Active
Bivalent
Negative
Pc-only
Trx-only
d
Numbers of DAEs in each category for the different CNCC subpopulations
Number of DAEs
0
40000
80000
120000
E8.5WT
FNP_E10.5WT
Mx_E10.5WT
Md_E10.5WT
PA2_E10.5WT
FNP_E11.5WT
Mx_E11.5WT
Md_E11.5WT
PA2_E11.5WT
DAE category
Active
Negative
Pc-marked
Primed
e
Pc−marked DAEs E8.5 WT
39% (3985)
61% (6329)
Pc−marked DAEs FNP_E10.5WT
50% (5479)
50% (5523)
Pc−marked DAEs Mx_E10.5WT
52% (4819)
48% (4390)
Pc−marked DAEs Md_E10.5WT
52% (4862)
48% (4409)
Pc−marked DAEs PA2_E10.5WT
54% (4983)
46% (4276)
Pc−marked DAEs FNP_E11.5WT
53% (5052)
47% (4396)
Pc−marked DAEs Mx_E11.5WT
52% (4754)
48% (4335)
Pc−marked DAEs Md_E11.5WT
55% (4832)
45% (3935)
Pc−marked DAEs PA2_E11.5WT
53% (4762)
47% (4702)
%
0
25
50
75
100
Pc−marked DAEs
H3K27me3+/H3K4me2−
H3K27me3+/H3K4me2+

Supplementary Figure 2: Classification of promoters and distal accessible elements in cranial neural crest cells

(**a**) Decision tree for classifying promoters (TSS +/-1kb) as active, Trx-only, bivalent, Pc-only or negative. Bivalent and Pc-only promoters are further categorized as Pc-marked. Classification is based on histone mark enrichment (H3K27ac, H3K27me3 and H3K4me2) and RNA expression levels. The (*) symbol indicates the strategy for classifying heterogeneously marked promoters (co-occurrence of H3K27ac and H3K27me3). (**b**) Flow-diagram for classifying Distal Accessible Elements (DAEs) into active, primed, Pc-marked or negative, based on histone mark enrichment (H3K27ac, H3K27me3 and H3K4me2). Pc-marked DAEs include Pc-only DAEs (H3K27me3+, H3K4me2-) and poised enhancers (H3K27me3+, H3K4me2+). The (*) symbol indicates the strategy for classifying heterogeneously marked DAEs (co-occurrence of H3K27ac and H3K27me3). (**c**-**d**) Bar-plots representing the number of promoters (**c**) and DAEs (**d**) in each category, in WT E8.5 pre-migratory progenitors and post-migratory CNCC subpopulations (frontonasal process, FNP; maxillary, Mx; mandibular, Md; and second pharyngeal arch, PA2) at E10.5 and E11.5. (**e**) Bar-plots showing the percentage of Pc-marked DAEs marked by both H3K27me3 and H3K4me2 (poised enhancers) compared to those marked by H3K27me3 only (H3K27me3+/H3K4me2-) in WT E8.5 pre-migratory progenitors and post-migratory CNCC subpopulations (FNP, Mx, Md and PA2) at E10.5 and E11.5.

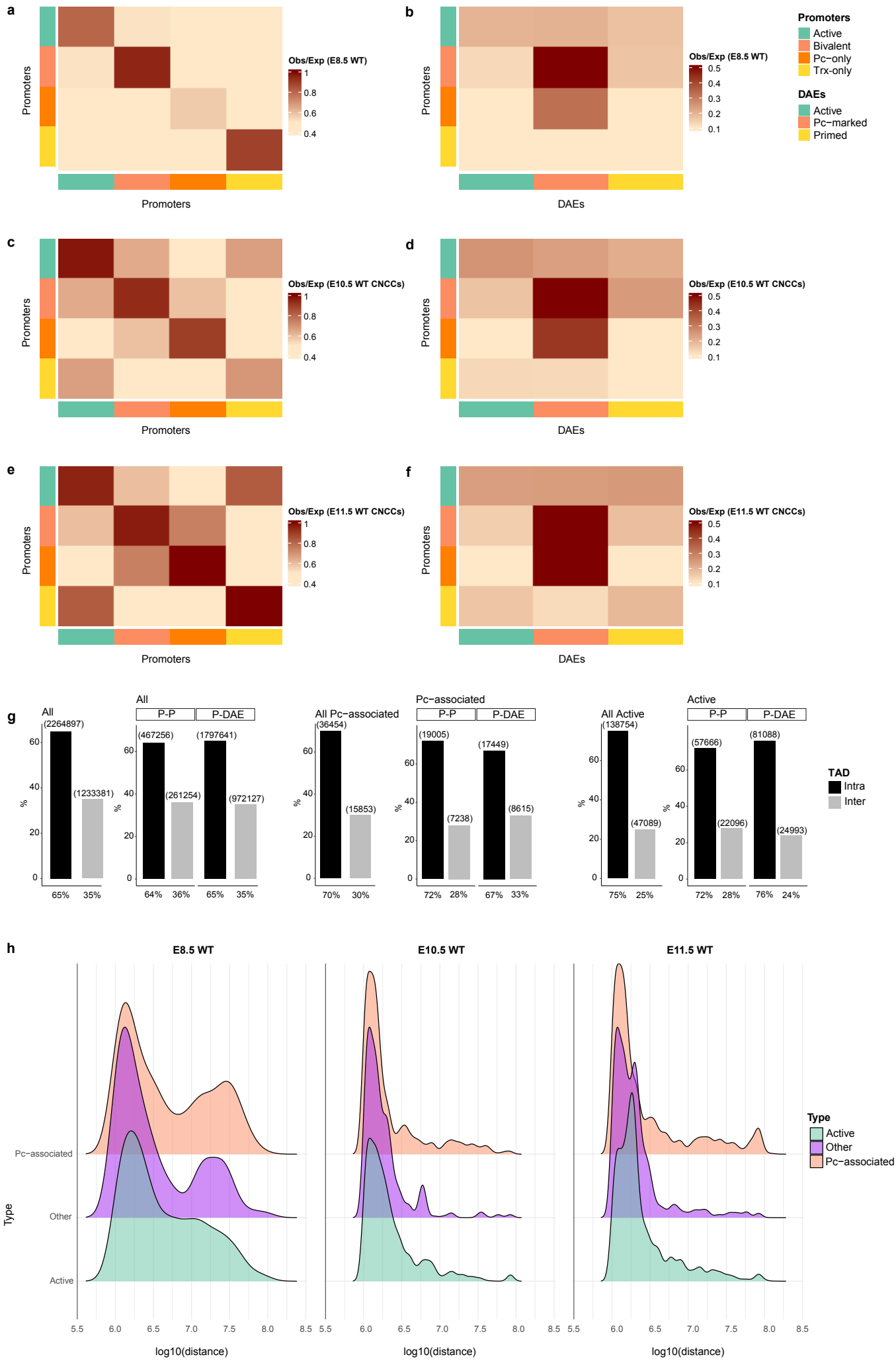

a
observed
mixture component 1
mixture component 2
model−based FDR
threshold = 0.48
threshold = 0.88
threshold = 0.36
Density
FDR
H3K27ac enrichment at TSS+/−1kb (log2)
H3K4me2 enrichment at TSS+/−1kb (log2)
H3K27me3 enrichment at TSS+/−1kb (log2)
b
c
d
e
E8.5 progenitors, WT
E10.5 Md CNCCs, WT
E10.5 PA2 CNCCs, WT
E11.5 Md CNCCs, WT
H3K27ac
H3K4me2
H3K27me3
asinh(RPKM)
active
bivalent
negative
Pc-only
Trx-only
Promoter state
Active
Bivalent (H3K27me3+ / H3K4me2+)
Negative
Pc (H3K27me3)-only
Trx (H3K4me2)-only

Supplementary Figure 3: Histone mark distribution for the different categories of promoters (**a**) Density distribution plots displaying the enrichment values of each histone mark at promoter regions, revealing a bimodal distribution. A two-component Gaussian mixture model with unequal variances was fitted to the median enrichment values across WT samples. Thresholds were determined at a false discovery rate (FDR) of 0.01. (**b-d**) Violin plots showing the distribution of H3K27ac (**b**), H3K4me2 (**c**) and H3K27me3 (**d**) for the different categories of promoters (active, Trx-only, bivalent, Pc-only and negative) in E8.5 WT pre-migratory progenitors, 10.5 WT mandibular (Md) and second pharyngeal arch (PA2) cranial neural crest cells (CNCCs) and E11.5 WT Md CNCCs. (**e**) Box plots showing the expression levels (asinh RPKM) of target genes, for each category of promoters.


a
observed
mixture component 1
mixture component 2
model−based FDR
threshold = 0.56
Density
FDR
H3K27ac enrichment at non−promoter ATAC peaks (log2)
threshold = 1.09
H3K4me2 enrichment at non−promoter ATAC peaks (log2)
threshold = 0.69
H3K27me3 enrichment at non−promoter ATAC peaks (log2)
b
E8.5 progenitors, WT
E10.5 FNP CNCCs, WT
E10.5 Mx CNCCs, WT
E11.5 FNP CNCCs, WT
H3K27ac
active
negative
Pc−marked
primed
Distal Accessible Element (DAE) state
Active
Negative
Pc−marked
Primed
c
H3K4me2
d
H3K27me3

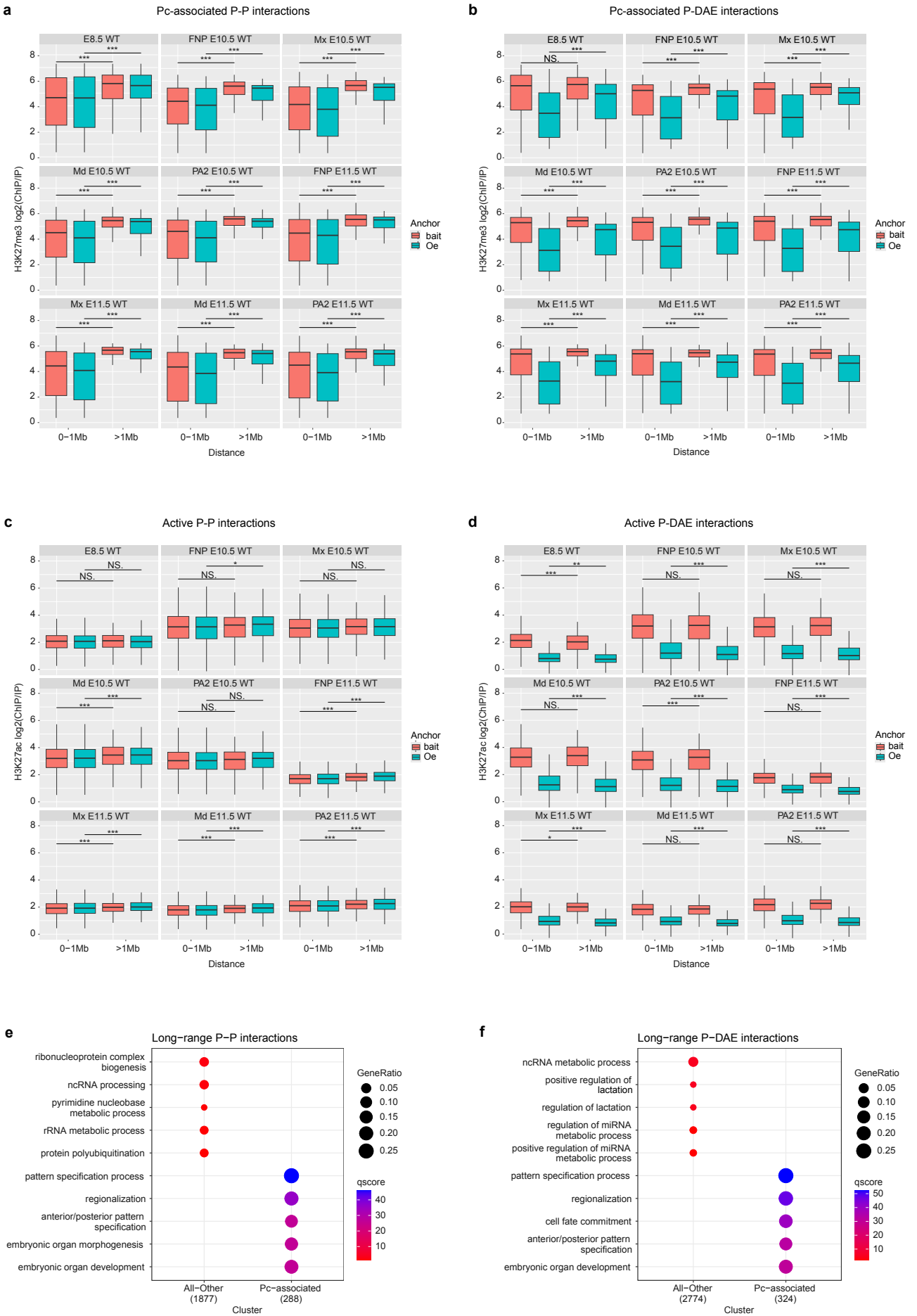
Supplementary Figure 4: Histone mark distribution for the different categories of distal accessible elements

(**a**) Density distribution plots displaying the enrichment values of each histone mark at non-promoter ATAC-seq peaks. A two-component Gaussian mixture model with unequal variances was fitted to the median enrichment values across WT samples. Thresholds were determined at a false discovery rate (FDR) of 0.05. (**b**-**d**) Violin plots showing the distribution of H3K27ac (**b**), H3K4me2 (**c**) and H3K27me3 (**d**) for the different categories of Distal Accessible Elements (DAEs) (active, primed, Pc-marked and negative) in E8.5 WT pre-migratory progenitors, 10.5 WT frontonasal (FNP) and maxillary (Mx) cranial neural crest cells (CNCCs) and E11.5 WT FNP CNCCs.


a
Promoters
Promoters
Obs/Exp (E8.5 WT)
1
0.8
0.6
0.4
b
Promoters
DAEs
Obs/Exp (E8.5 WT)
0.5
0.4
0.3
0.2
0.1
Promoters
Active
Bivalent
Pc−only
Trx−only
DAEs
Active
Pc−marked
Primed
c
Promoters
Promoters
Obs/Exp (E10.5 WT CNCCs)
1
0.8
0.6
0.4
d
Promoters
DAEs
Obs/Exp (E10.5 WT CNCCs)
0.5
0.4
0.3
0.2
0.1
e
Promoters
Promoters
Obs/Exp (E11.5 WT CNCCs)
1
0.8
0.6
0.4
f
Promoters
DAEs
Obs/Exp (E11.5 WT CNCCs)
0.5
0.4
0.3
0.2
0.1
g
All
(2264897)
(1233381)
65%
35%
All
P-P
P-DAE
(467256)
(261254)
(1797641)
(972127)
64%
36%
65%
35%
All Pc−associated
(36454)
(15853)
70%
30%
Pc−associated
P-P
P-DAE
(19005)
(7238)
(17449)
(8615)
72%
28%
67%
33%
All Active
(138754)
(47089)
75%
25%
Active
P-P
P-DAE
(57666)
(22096)
(81088)
(24993)
72%
28%
76%
24%
%
TAD
Intra
Inter
h
E8.5 WT
E10.5 WT
E11.5 WT
Pc−associated
Other
Active
Type
5.5
6.0
6.5
7.0
7.5
8.0
8.5
log10(distance)
Type
Active
Other
Pc−associated

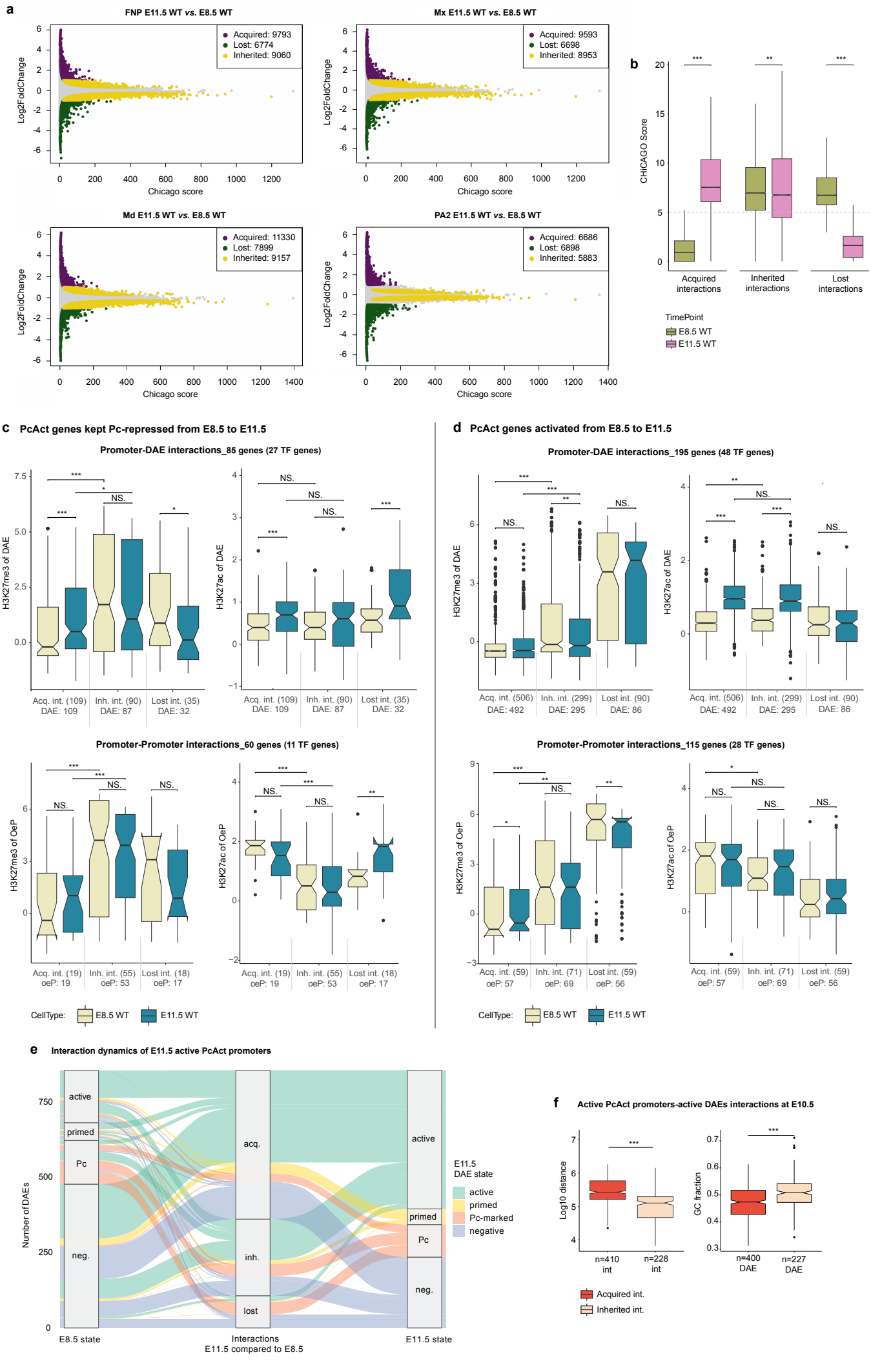
Supplementary Figure 5: Polycomb-dependent long-range chromatin interactions

(**a**-**f**) Correlation plots for Promoter-Promoter (P-P) (**a**, **c**, **e**) and Promoter-Distal Accessible Element (P-DAE) (**b**, **d**, **f**) interactions, depicted as heatmaps showing the ratio of observed to expected interaction probabilities in E8.5 WT pre-migratory progenitors (**a**, **b**) and in E10.5 (**c**, **d**) and E11.5 (**e**, **f**) WT post-migratory cranial neural crest cells (CNCCs). Data from E10.5 and E11.5 CNCCs subpopulations have been merged, respectively. (**g**) Bar-plots showing the ratio of intra-TAD vs. inter-TAD interactions for all interactions (**left**), Pc-associated interactions (both ends Pc-marked, **middle**), and active interactions (both ends active, **right**). Data from E8.5/E10.5/E11.5 WT CNCCs were merged. (**h**) Density plots showing the distance distribution of different interaction types in E8.5 WT pre-migratory progenitors and in E10.5/E11.5 WT post-migratory CNCCs (with data from E10.5 and E11.5 CNCCs subpopulations merged separately). The plots display three interaction types: active, Pc-associated and other (interactions that do not fall into the above two categories). Distances greater than 1Mb were retained to improve visualization. The plots reveal that Pc-associated interactions tend to span longer distances than active and other interactions, particularly at E8.5, while remaining detectable at later stages (E10.5 and E11.5).


a
Pc-associated P-P interactions
b
Pc-associated P-DAE interactions
E8.5 WT
FNP E10.5 WT
Mx E10.5 WT
Md E10.5 WT
PA2 E10.5 WT
FNP E11.5 WT
Mx E11.5 WT
Md E11.5 WT
PA2 E11.5 WT
H3K27me3 log2(ChIP/IP)
Anchor
bait
Oe
0−1Mb
>1Mb
Distance
c
Active P-P interactions
d
Active P-DAE interactions
H3K27ac log2(ChIP/IP)
e
Long−range P−P interactions
ribonucleoprotein complex biogenesis
ncRNA processing
pyrimidine nucleobase metabolic process
rRNA metabolic process
protein polyubiquitination
pattern specification process
regionalization
anterior/posterior pattern specification
embryonic organ morphogenesis
embryonic organ development
GeneRatio
qscore
All−Other (1877)
Pc−associated (288)
Cluster
f
Long−range P−DAE interactions
ncRNA metabolic process
positive regulation of lactation
regulation of lactation
regulation of miRNA metabolic process
positive regulation of miRNA metabolic process
pattern specification process
regionalization
cell fate commitment
anterior/posterior pattern specification
embryonic organ development
All−Other (2774)
Pc−associated (324)
Cluster

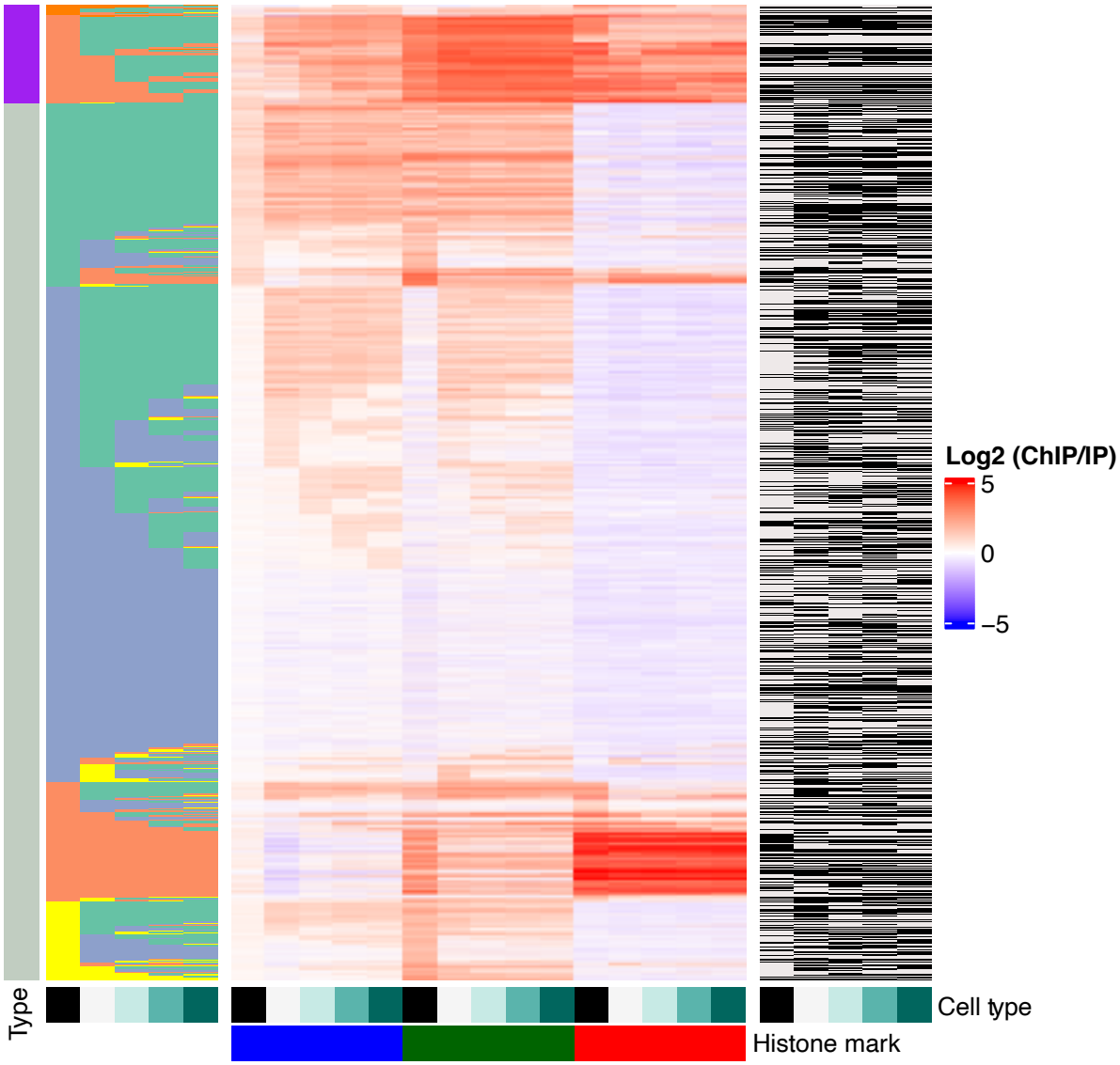
Supplementary Figure 6: Enrichment of histone marks in long-range chromatin interactions and gene ontology analysis

(**a**-**d**) Box plots showing H3K27me3 (**a**, **b**) and H3K27ac (**c**, **d**) enrichment (at bait and other-end (Oe) anchors), for Promoter-Promoter (P-P) (**a**, **c**) and Promoter-Distal Accessible Element (P-DAE) (**b**, **d**) interactions. Comparisons are made between 0-1Mb and >1Mb interactions in WT E8.5 pre-migratory progenitors and E10.5/E11.5 post-migratory cranial neural crest cell (CNCC) subpopulations (frontonasal process, FNP; maxillary, Mx; mandibular, Md and second pharyngeal arch, PA2). Box plots indicate median (middle line), interquartile range (IQR; box) and whiskers extending to 1.5×IQR. P-value: two-sided Wilcoxon rank-sum test (***, $p \leq 0.001$; **, $p \leq 0.01$; *, $p \leq 0.05$; NS., $p > 0.05$). (**e**-**f**) Gene Ontology (GO) analysis of genes involved in >1Mb P-P (**e**) and P-DAE (**f**) interactions, comparing Pc-associated interactions versus all-other interactions. The analysis highlights significant enrichment for GO terms related to cranial neural crest cell (CNCC) differentiation, including 'pattern specification process' and 'regionalization' for Pc-associated interactions.


a
FNP E11.5 WT vs. E8.5 WT
Acquired: 9793
Lost: 6774
Inherited: 9060
Mx E11.5 WT vs. E8.5 WT
Acquired: 9593
Lost: 6698
Inherited: 8953
Md E11.5 WT vs. E8.5 WT
Acquired: 11330
Lost: 7899
Inherited: 9157
PA2 E11.5 WT vs. E8.5 WT
Acquired: 6686
Lost: 6898
Inherited: 5883
Log2FoldChange
Chicago score
b
CHiCAGO Score
Acquired interactions
Inherited interactions
Lost interactions
TimePoint
E8.5 WT
E11.5 WT
c
PcAct genes kept Pc-repressed from E8.5 to E11.5
Promoter-DAE interactions_85 genes (27 TF genes)
H3K27me3 of DAE
H3K27ac of DAE
Acq. int. (109) DAE: 109
Inh. int. (90) DAE: 87
Lost int. (35) DAE: 32
Promoter-Promoter interactions_60 genes (11 TF genes)
H3K27me3 of OeP
H3K27ac of OeP
Acq. int. (19) oeP: 19
Inh. int. (55) oeP: 53
Lost int. (18) oeP: 17
CellType: E8.5 WT E11.5 WT
d
PcAct genes activated from E8.5 to E11.5
Promoter-DAE interactions_195 genes (48 TF genes)
Acq. int. (506) DAE: 492
Inh. int. (299) DAE: 295
Lost int. (90) DAE: 86
Promoter-Promoter interactions_115 genes (28 TF genes)
Acq. int. (59) oeP: 57
Inh. int. (71) oeP: 69
Lost int. (59) oeP: 56
CellType: E8.5 WT E11.5 WT
e
Interaction dynamics of E11.5 active PcAct promoters
Number of DAEs
active
primed
Pc
neg.
acq.
inh.
lost
E8.5 state
Interactions E11.5 compared to E8.5
E11.5 state
E11.5 DAE state
active
primed
Pc-marked
negative
f
Active PcAct promoters-active DAEs interactions at E10.5
Log10 distance
n=410 int
n=228 int
GC fraction
n=400 DAE
n=227 DAE
Acquired int.
Inherited int.

Supplementary Figure 7: Mapping chromatin interaction dynamics in cranial neural crest cells

(**a**) MA (mean-average) plots showing acquired (purple), lost (green) and inherited (yellow) interactions in E11.5 WT frontonasal (FNP), maxillary (Mx), mandibular (Md) and second pharyngeal arch (PA2) cranial neural crest cells (CNCCs), compared with E8.5 WT progenitors (see methods). (**b**) Box plots comparing interactions strengths (CHiCAGO score) of acquired, inherited and lost interactions between E11.5 WT post-migratory CNCCs and E8.5 WT pre-migratory progenitors. Data from E11.5 WT FNP, Mx, Md and PA2 subpopulations were merged. (**c-d**) Box plots showing H3K27me3 and H3K27ac enrichment at the other end (Oe) – either Distal Accessible Elements (DAEs) (**top**) or promoters (OeP) (**bottom**) – for Promoter-DAE (P-DAE) and Promoter-Promoter (P-P) interactions, involving PcAct promoters that either remain Pc-repressed (**c**) or have switched to active (**d**) in E11.5 WT post-migratory CNCCs. Interactions were extracted from each E11.5 prominence (FNP, Mx, Md, PA2), and then separately merged. For each interaction type (acquired (Acq), inherited (Inh) and lost), the number of interactions is indicated. Below these numbers, the number of unique DAEs involved in P-DAE interactions (**top**) and the number of unique OeP involved in P-P interactions (**bottom**) are also shown. (**e**). Sankey (alluvial) diagram depicting chromatin-state and interaction dynamics (from E8.5 to E11.5) of the DAEs interacting with active PcAct promoters at E11.5. Flows width is proportional to the number of DAEs following each trajectory. Strata labels indicate chromatin states of DAEs at each developmental stage (left, E8.5; right, E11.5) and interaction type (acquired (acq.), inherited (inh.) or lost) from E8.5 to E11.5. Flows are colored by the epigenetic state of DAEs at E11.5. (**f**) Boxplots showing interaction distance (log10) between active PcAct promoters and active DAEs in E10.5 CNCCs (**left**) and GC content of the involved unique DAEs (**right**), comparing acquired and inherited interactions. In **b**, **c**, **d** and **f**, box plots indicate median (middle line), interquartile range (IQR; box) and whiskers extending to 1.5×IQR. In **c**, **d** and **f**, single points indicate outliers. P-value: two-sided Wilcoxon rank-sum test (***, $p \leq 0.001$; **, $p \leq 0.01$; *, $p \leq 0.05$; NS., $p > 0.05$).



Cell type
- Progenitors_E8.5_WT
- FNP_E10.5_WT
- Mx_E10.5_WT
- Md_E10.5_WT
- PA2_E10.5_WT

Type
- Promoter
- DAE

Categories

Promoters
- Pc−only
- Bivalent
- Active

DAEs
- Negative
- Primed
- Active
- Pc−marked

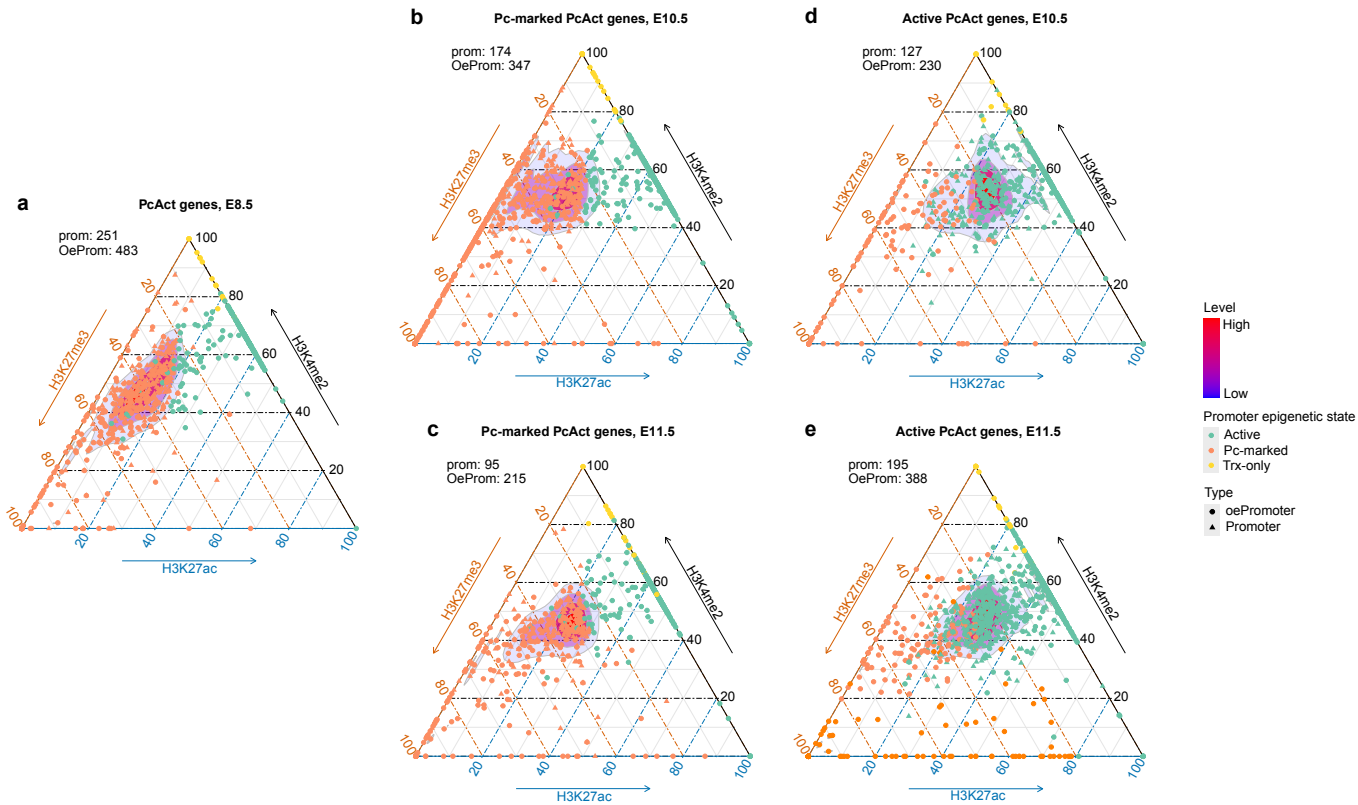
Histone mark
- H3K27ac
- H3K4me2
- H3K27me3

Any Interaction
- TRUE
- FALSE

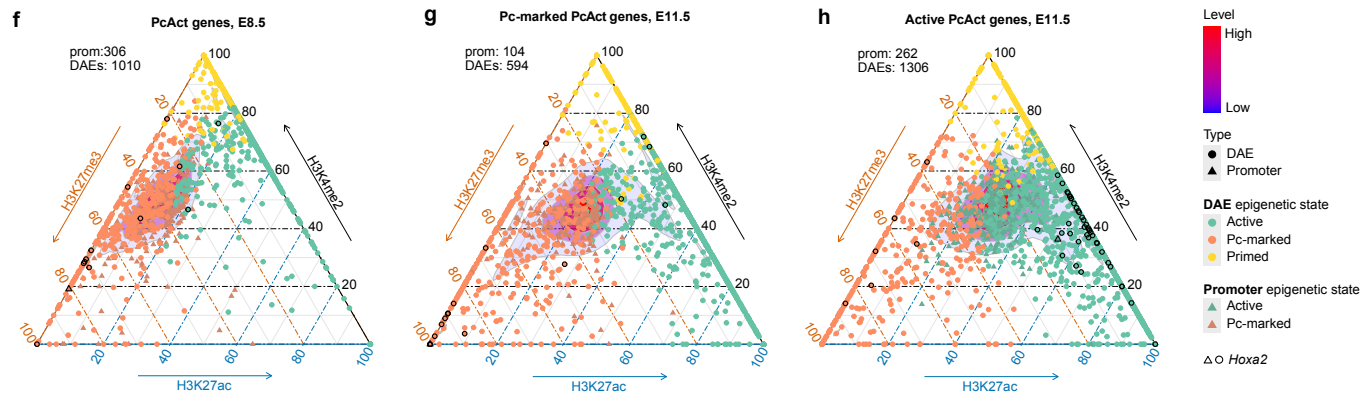
Supplementary Figure 8: Integrated heat map of PcAct genes and interacting DAEs across neural crest cell subpopulations.

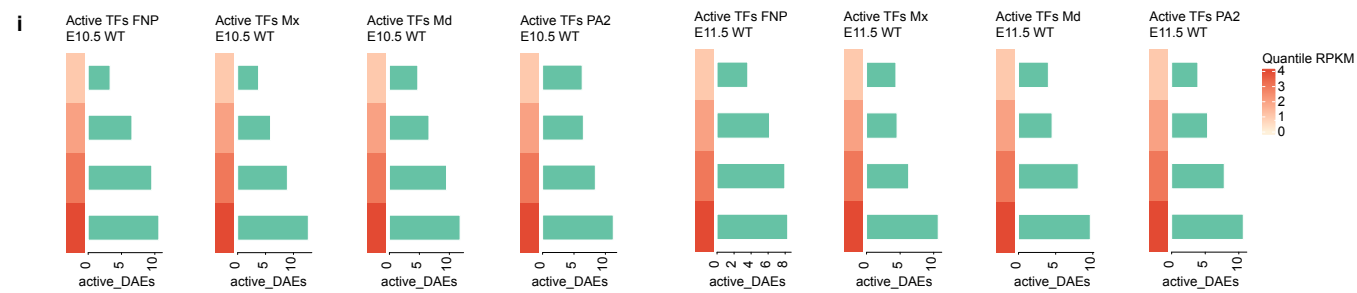
Heat map integrating epigenetic classification, histone mark enrichment profiles, and chromatin interaction status at PcAct genes and their associated distal accessible elements (DAEs) in E8.5 pre-migratory progenitors and E10.5 post-migratory cranial neural crest cell (CNCC) subpopulations (frontonasal process (FNP), maxillary (Mx), mandibular (Md), and second pharyngeal arch (PA2)). Histone mark enrichment is shown at both PcAct gene promoters and their associated DAEs, together with a binary interaction status (TRUE/FALSE) indicating whether promoters or DAEs participate in detectable chromatin interactions. TRUE interactions are defined by a CHiCAGO score ≥ 5.

Promoter - promoter interactions



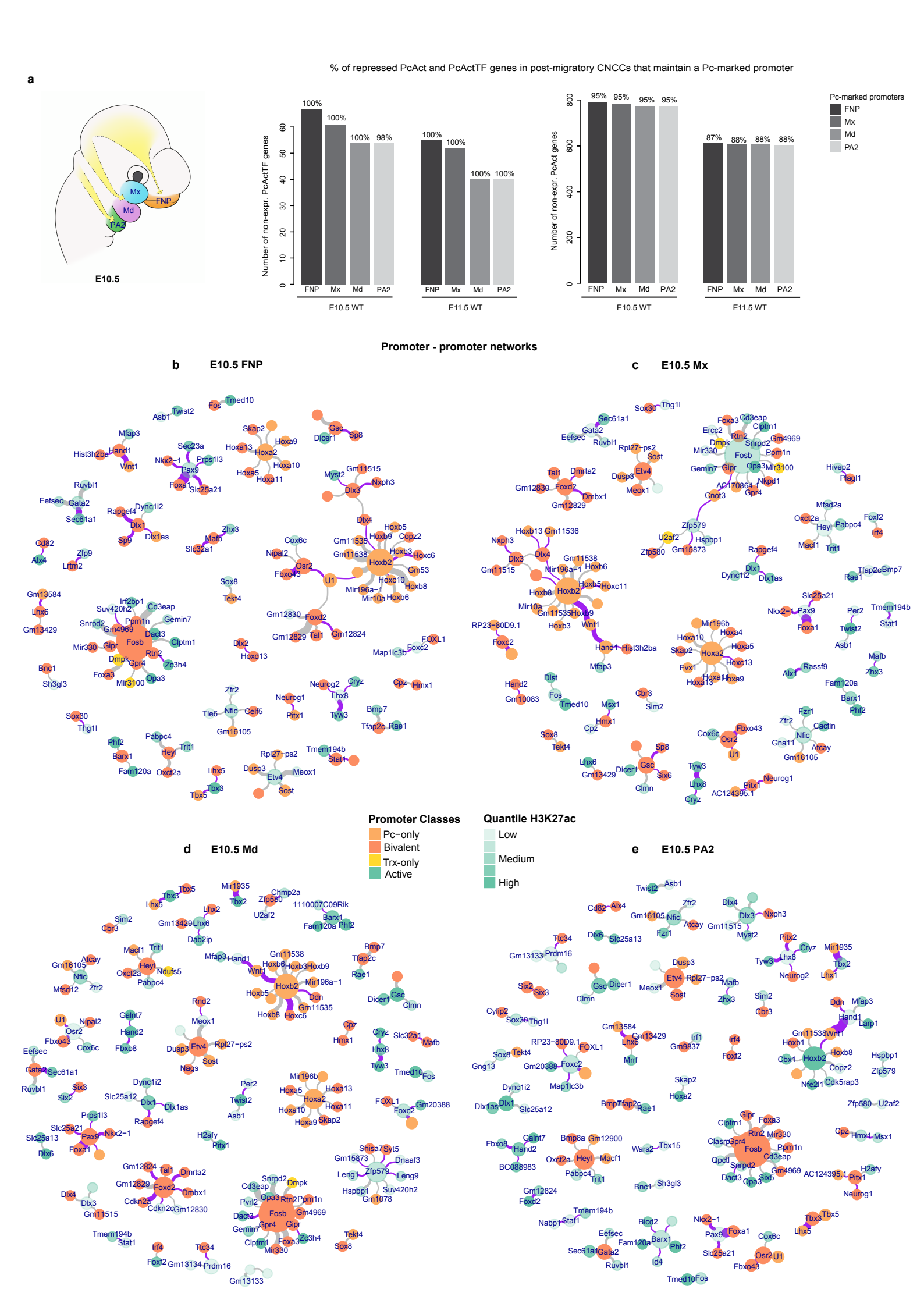
Promoter - DAE interactions





Supplementary Figure 9: Comparative analysis of PcAct promoter interactions from pre- to post-migratory stages, based on their epigenetic state in post-migratory cranial neural crest cells

(**a**-**e**) Ternary plots showing the relative enrichment of H3K27me3, H3K27ac, and H3K4me2 at PcAct promoters and interacting other-end promoters (OeP) in WT E8.5 pre-migratory progenitors (**a**) and in WT E10.5 and E11.5 cranial neural crest cells (CNCCs) (**b**-**e**), where promoters remain Pc-repressed (**b**, **c**) or become active (**d**, **e**) (see Methods). (**f**-**h**) Ternary plots of PcAct promoters and their interacting Distal Accessible Elements (DAEs) in WT E8.5 pre-migratory progenitors (**f**) and E11.5 CNCCs (**g**, **h**), where promoters remain Pc-repressed (**g**) or become active (**h**) (see Methods). The *Hoxa2* promoter and its interacting DAEs are outlined (black). The outlined promoter and interacting DAEs in (**g**) were randomly selected from CNCC subpopulations, where *Hoxa2* remains Pc-repressed. In **a** to **h**, colors indicate epigenetic categories of promoters (triangles) and DAEs (dots), with spatial density gradients highlighting overall distribution. (**i**) Bar plot showing the mean number of active DAEs (green bars) interacting with active promoters of transcription-factor (TF) encoding genes, grouped into four quantiles (red) according to their gene expression levels (Quantile RPKM), in the different E10.5 and E11.5 CNCC subpopulations.

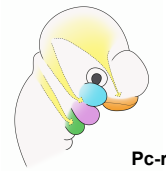

a
% of repressed PcAct and PcActTF genes in post-migratory CNCCs that maintain a Pc-marked promoter
Mx
FNP
Md
PA2
E10.5
Number of non-expr. PcActTF genes
100%
100%
100%
98%
100%
100%
100%
100%
FNP
Mx
Md
PA2
E10.5 WT
E11.5 WT
Number of non-expr. PcAct genes
95%
95%
95%
95%
87%
88%
88%
88%
Pc-marked promoters
FNP
Mx
Md
PA2
Promoter - promoter networks
b E10.5 FNP
c E10.5 Mx
Promoter Classes
Pc−only
Bivalent
Trx-only
Active
Quantile H3K27ac
Low
Medium
High
d E10.5 Md
e E10.5 PA2

Supplementary Figure 10: Promoter-promoter interaction networks of PcActTF promoters in E10.5 cranial neural crest cell subpopulations

(**a**) (**left**) Schematic of an E10.5 embryo, showing the migration pattern of cranial neural crest cells (CNCCs) (yellow arrows) into the facial prominences, highlighted in orange (frontonasal process, FNP), blue (maxillary, Mx), purple (mandibular, Md) and green (second pharyngeal arch, PA2). (**Right**) Bar plots showing the percentage of PcAct and PcActTF promoters that remained Pc-marked in the E10.5 and E11.5 CNCC subpopulations where they are maintained transcriptionally repressed. (**b**-**e**) Promoter-Promoter (P-P) interaction networks of PcActTF promoters that display at least one significant interaction (CHiCAGO score ≥ 5) in E10.5 FNP, Mx, Md and PA2 CNCC subpopulations. Nodes represent promoters. Node size reflects connectivity, and node color indicates the epigenetic state of promoters. Active promoters are further distinguished by green transparency, based on their quantile acetylation levels. Edge thickness corresponds to interaction strength. Purple edges indicate inter-TAD interactions. Empty nodes mark removed *Rik* genes; negative promoters and DAEs are excluded (see Methods).



E8.5 pre-migratory progenitors



E10.5 post-migratory CNCCs

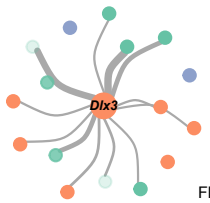
PcAct genes (poised)

Pc-repressed

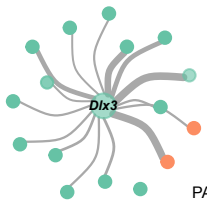
Activated

Dlx3

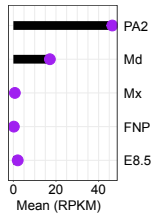




FNP

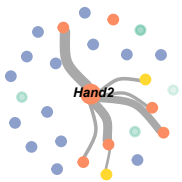


PA2

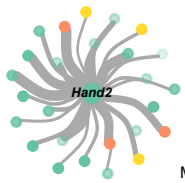


Hand2

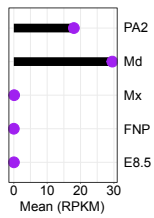




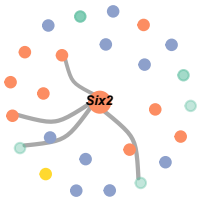
FNP

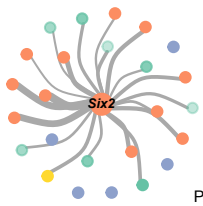


Md

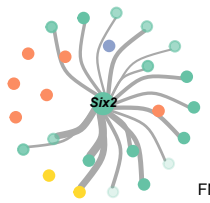


Six2

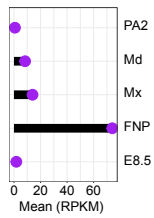




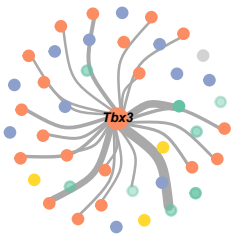
PA2

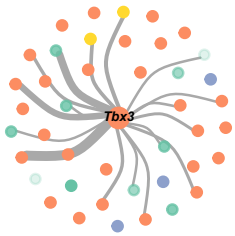


FNP

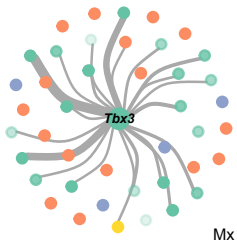


Tbx3

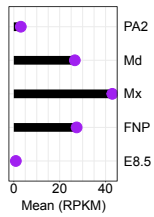




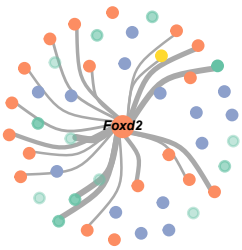
PA2

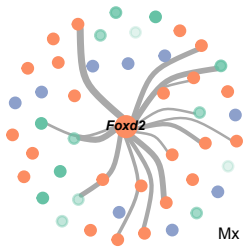


Mx

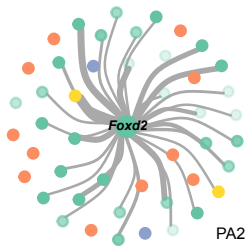


Foxd2

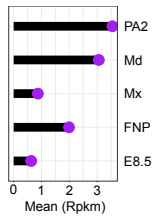




Mx



PA2



Epigenetic state

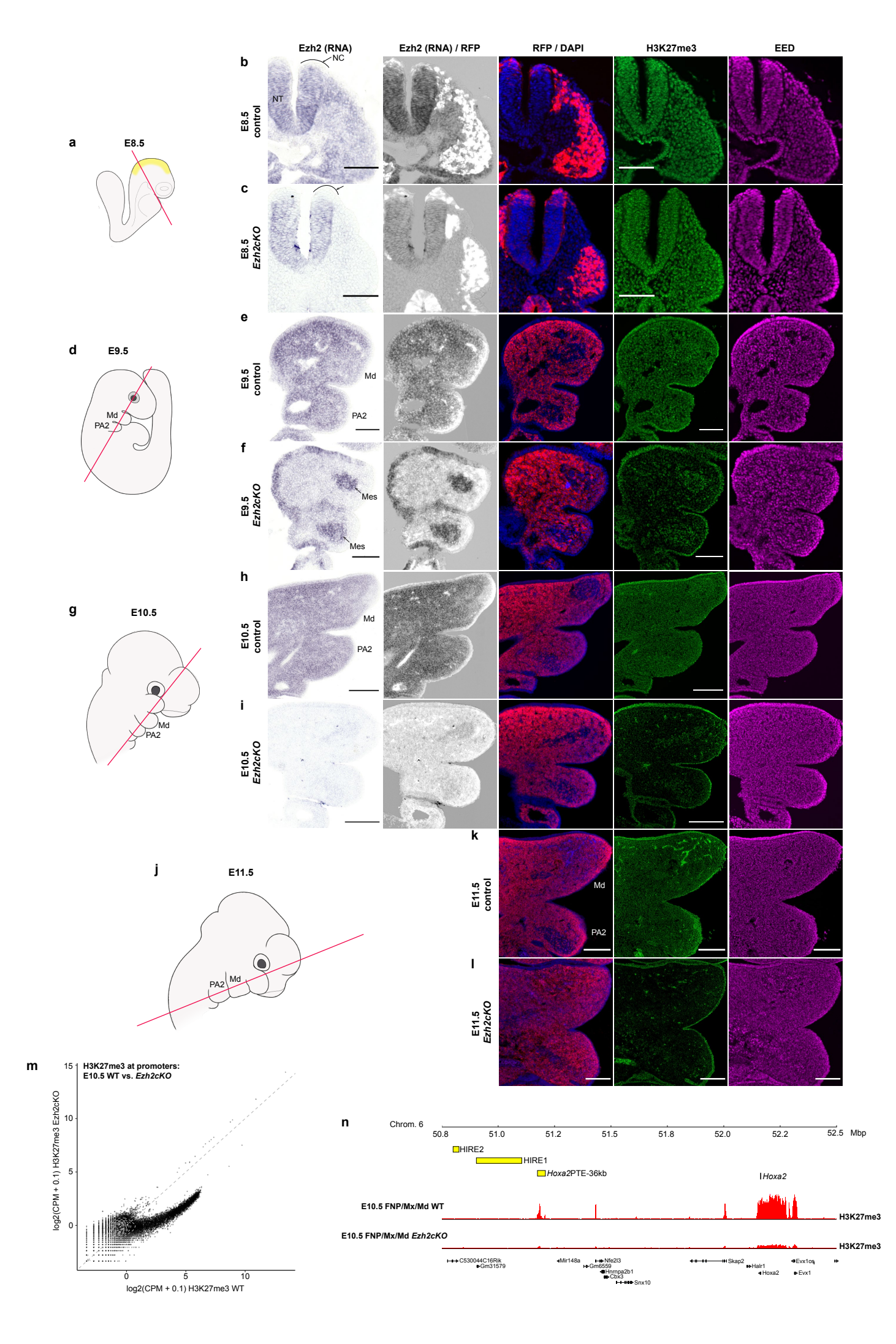
Promoters
- Bivalent
- Active

DAEs
- Pc-marked
- Primed
- Active
- Negative
- Not assigned

Quantile H3K27ac
- Low
- Medium
- High

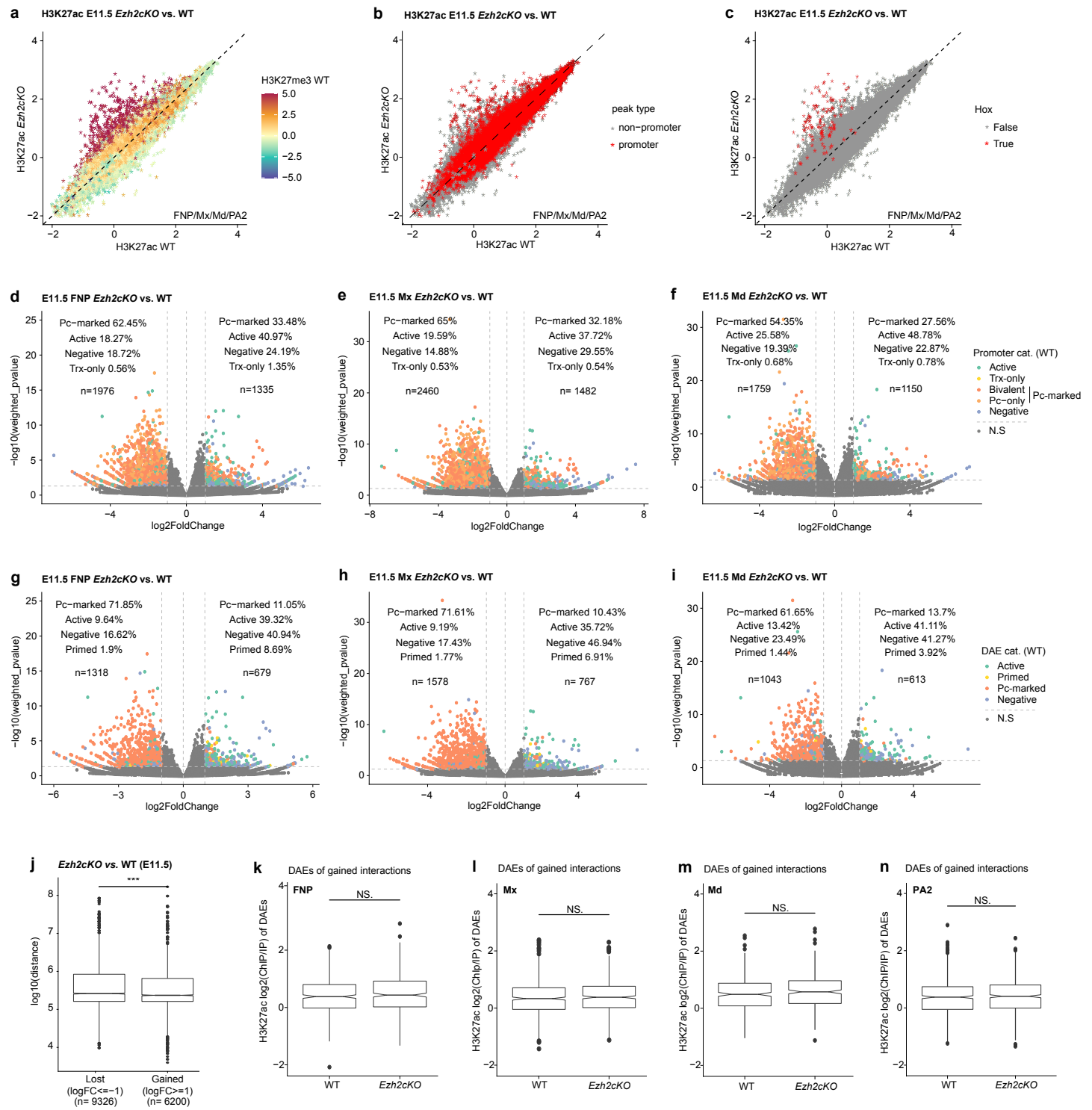
Supplementary Figure 11: Spatiotemporal dynamics of P-DAE chromatin interactions at representative PcAct promoters during craniofacial development

Promoter-Distal Accessible Element (P-DAE) interaction networks for representative PcActTF promoters in E8.5 pre-migratory progenitors (**left**) and E10.5 post-migratory cranial neural crest cell (CNCC) sub-populations, where promoters remain Pc-repressed (**middle**) or become active (**right**). Central nodes represent promoters; surrounding nodes represent DAEs. Node colors indicate the epigenetic state of promoters and DAEs, with active promoters and DAEs also displaying a green transparency according to their quantile acetylation levels. Edge thickness denotes interaction strength. DAEs spatial coordinates are conserved across cell populations and stages, non-interacting DAEs appear unconnected (see Methods). Expression levels in E8.5 progenitors and E10.5 CNCC subpopulations (frontonasal, (FNP), maxillary (Mx), mandibular (Md) and second pharyngeal arch (PA2)) are shown on the right.


Ezh2 (RNA)
Ezh2 (RNA) / RFP
RFP / DAPI
H3K27me3
EED
a
E8.5
b
E8.5 control
NC
NT
c
E8.5 Ezh2cKO
d
E9.5
Md
PA2
e
E9.5 control
f
E9.5 Ezh2cKO
Mes
g
E10.5
h
E10.5 control
i
E10.5 Ezh2cKO
j
E11.5
k
E11.5 control
l
E11.5 Ezh2cKO
m
H3K27me3 at promoters:
E10.5 WT vs. Ezh2cKO
log2(CPM + 0.1) H3K27me3 Ezh2cKO
log2(CPM + 0.1) H3K27me3 WT
n
Chrom. 6
50.8
51.0
51.2
51.5
51.8
52.0
52.2
52.5 Mbp
HIRE2
HIRE1
Hoxa2PTE-36kb
Hoxa2
E10.5 FNP/Mx/Md WT
H3K27me3
E10.5 FNP/Mx/Md Ezh2cKO
H3K27me3
C530044C16Rik
Gm31579
Mir148a
Nfe2l3
Gm6559
Hnrnpa2b1
Cbx3
Snx10
Skap2
Halr1
Hoxa2
Evx1os
Evx1

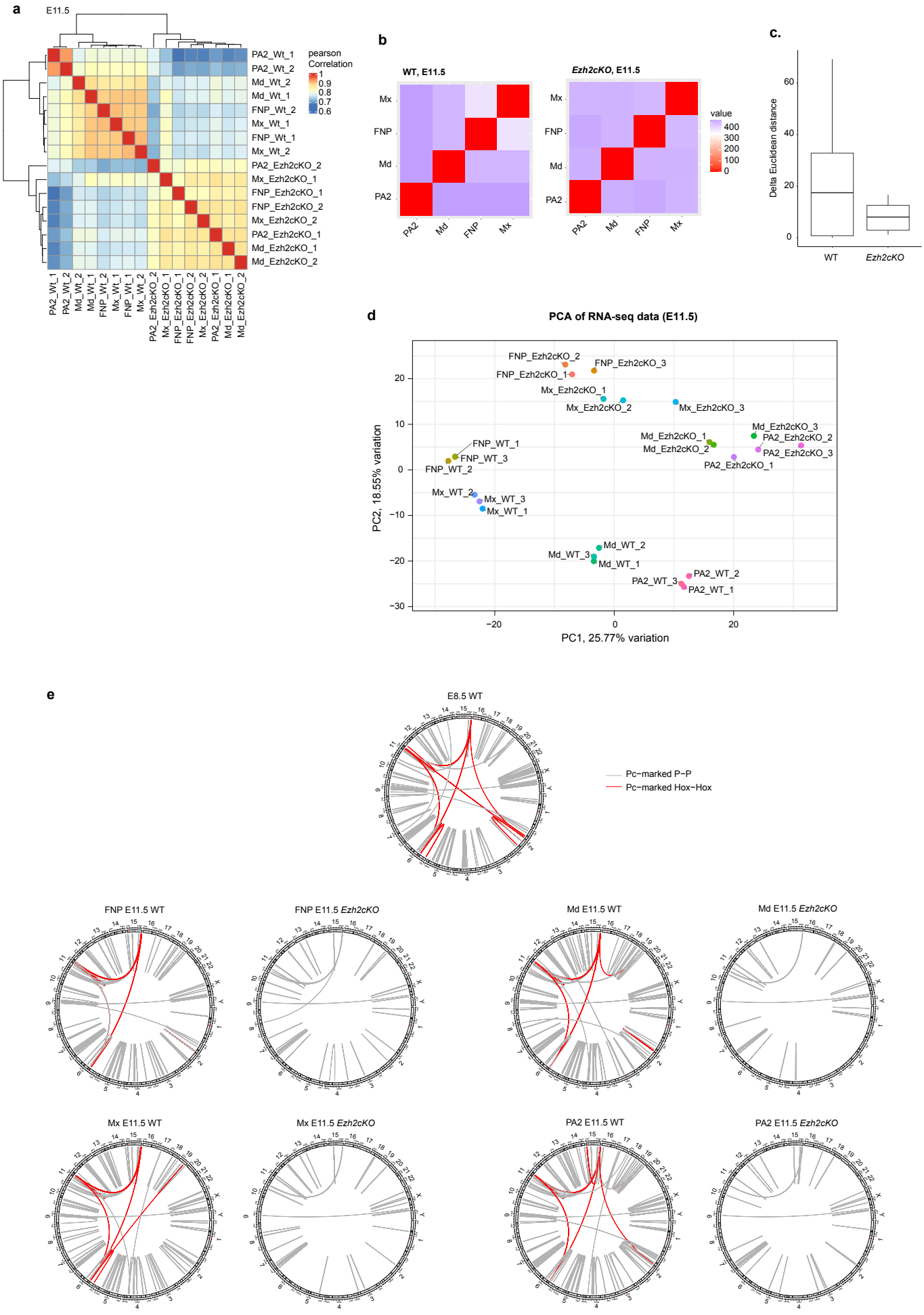
Supplementary Figure 12: Time-course analysis of H3K27me3 loss in *Ezh2cKO* cranial neural crest cells

(**a**) Schematic of an E8.5 embryo indicating the planes of section corresponding to the images shown in (**b**, **c**). (**b**, **c**) From left to right, panels show: *in situ* hybridization on sections using an *Ezh2* antisense probe; *Ezh2 in situ* hybridization combined with anti-RFP immunostaining; anti-RFP immunostaining with DAPI counterstaining; anti-H3K27me3 immunostaining; and anti-EED immunostaining in E8.5 control (i.e., *Wnt1::Cre; RosaRFP*) (**b**) and *Ezh2cKO* (i.e., *Wnt1::Cre;ROSA*^{RFP}*;Ezh2*$^{flox/flox}$) (**c**) embryos. (**d**-**l**) Similar to (**a**-**c**) but at E9.5 (**d**-**f**), E10.5 (**g**-**i**) and E11.5 (**j**-**l**). For each row, the three leftmost panels show *Ezh2 in situ* hybridization, anti-RFP immunostaining, and DAPI counterstaining on the same sections, whereas the two rightmost panels show anti-H3K27me3 and anti-EED immunostaining performed on the same sections, distinct from those shown in the three leftmost panels. Mes, mesoderm; NC, neural crest; NT, neural tube; Md, mandibular process; PA2, second pharyngeal arch. Scale bars in E8.5 and E9.5 embryos represent 100 μm. Scale bars in E10.5 and E11.5 embryos represent 200 μm. (**m**) Scatter plot showing the correlation of H3K27me3 ChIP enrichment (log2 (CPM + 0.1)) at promoters in E10.5 WT (x axis) and *Ezh2cKO* (y axis) frontonasal (FNP), maxillary (Mx) and mandibular (Md) merged cranial neural crest cell (CNCCs). (**n**) Genome browser view of chromosome 6 (50,500,000–52,500,000) showing ChIP-seq profiles for H3K27me3 in the FNP/Mx/Md merged CNCCs in E10.5 WT and *Ezh2cKO* embryos. For better readability, genomic coordinates within the *Hoxa* cluster only show *Hoxa2* genomic position.


a
H3K27ac E11.5 Ezh2cKO vs. WT
H3K27ac Ezh2cKO
H3K27ac WT
FNP/Mx/Md/PA2
H3K27me3 WT
5.0
2.5
0.0
−2.5
−5.0
b
H3K27ac E11.5 Ezh2cKO vs. WT
peak type
non−promoter
promoter
c
H3K27ac E11.5 Ezh2cKO vs. WT
Hox
False
True
d
E11.5 FNP Ezh2cKO vs. WT
Pc−marked 62.45%
Active 18.27%
Negative 18.72%
Trx-only 0.56%
n=1976
Pc−marked 33.48%
Active 40.97%
Negative 24.19%
Trx-only 1.35%
n=1335
−log10(weighted_pvalue)
log2FoldChange
e
E11.5 Mx Ezh2cKO vs. WT
Pc−marked 65%
Active 19.59%
Negative 14.88%
Trx-only 0.53%
n=2460
Pc−marked 32.18%
Active 37.72%
Negative 29.55%
Trx-only 0.54%
n= 1482
f
E11.5 Md Ezh2cKO vs. WT
Pc−marked 54.35%
Active 25.58%
Negative 19.39%
Trx-only 0.68%
n=1759
Pc−marked 27.56%
Active 48.78%
Negative 22.87%
Trx-only 0.78%
n=1150
Promoter cat. (WT)
Active
Trx-only
Bivalent
Pc-only
Pc-marked
Negative
N.S
g
E11.5 FNP Ezh2cKO vs. WT
Pc−marked 71.85%
Active 9.64%
Negative 16.62%
Primed 1.9%
n=1318
Pc−marked 11.05%
Active 39.32%
Negative 40.94%
Primed 8.69%
n=679
h
E11.5 Mx Ezh2cKO vs. WT
Pc−marked 71.61%
Active 9.19%
Negative 17.43%
Primed 1.77%
n= 1578
Pc−marked 10.43%
Active 35.72%
Negative 46.94%
Primed 6.91%
n= 767
i
E11.5 Md Ezh2cKO vs. WT
Pc−marked 61.65%
Active 13.42%
Negative 23.49%
Primed 1.44%
n=1043
Pc−marked 13.7%
Active 41.11%
Negative 41.27%
Primed 3.92%
n=613
DAE cat. (WT)
Active
Primed
Pc-marked
Negative
N.S
j
Ezh2cKO vs. WT (E11.5)
***
log10(distance)
Lost
(logFC<=−1)
(n= 9326)
Gained
(logFC>=1)
(n= 6200)
k
DAEs of gained interactions
FNP
NS.
H3K27ac log2(ChIP/IP) of DAEs
WT
Ezh2cKO
l
DAEs of gained interactions
Mx
NS.
m
DAEs of gained interactions
Md
NS.
n
DAEs of gained interactions
PA2
NS.

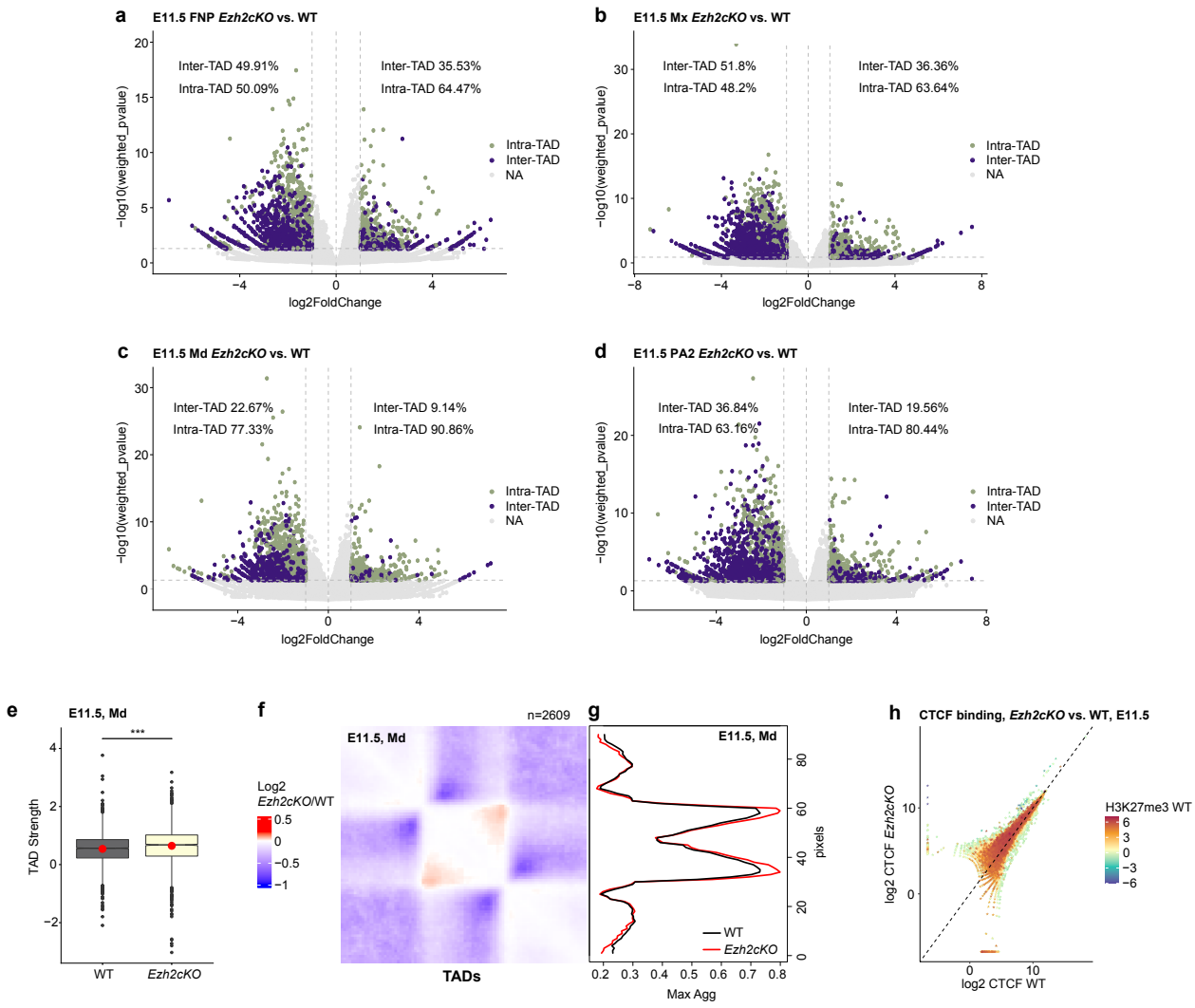
Supplementary Figure 13: Epigenetic states of promoters and DAEs associated with altered chromatin interactions in *Ezh2cKO* cranial neural crest cells

(**a** to **c**) Scatter plots of ATAC-seq peaks, comparing H3K27ac enrichment in E11.5 WT (x axis) vs. *Ezh2cKO* (y axis) in merged frontonasal (FNP), maxillary (Mx), mandibular (Md) and second pharyngeal arch (PA2) cranial neural crest cells (CNCCs). Color codes represent H3K27me3 enrichment in WT CNCCs (**a**), peak type (**b**), and whether the peak belongs to a Hox cluster (**c**). (**d** to **i**) Volcano plots of differential Promoter - Distal Accessible Elements (P-DAE) interactions between E11.5 *Ezh2cKO* and WT CNCCs, in FNP (**d**, **g**), Mx (**e**, **h**) and Md (**f**, **i**). Points represent interactions, colored by promoter (**d**, **e**, **f**) or DAE (**g**, **h**, **i**) epigenetic state. Significant interactions (weighted p-value ≤ 0.05, $|\text{LogFC}| \geq 1$ are indicated by dashed grey lines; percentages show category proportions. Non-classified (NA) promoters and DAEs were separately excluded from their respective plots. (**j**) Box plot comparing the log10 distance distribution of lost (n=9326) vs. gained (n=6200) interactions in E11.5 *Ezh2cKO* CNCCs relative to WT; data from FNP, Mx, Md and PA2 CNCCs were merged for the analysis. The plot shows that gained interactions in *Ezh2cKO* CNCCs are shorter-range compared to lost ones. (**k**-**n**) Box plots showing H3K27ac enrichments at DAEs involved in gained interactions in *Ezh2cKO* CNCCs, comparing E11.5 *Ezh2cKO* and WT CNCC subpopulations (FNP, Mx, Md and PA2). No significant increase in H3K27ac enrichment is observed at DAEs associated with gained interactions in *Ezh2cKO* CNCCs. In **j**-**n**, box plots indicate median (middle line), interquartile range (IQR; box) and whiskers extending to 1.5×IQR. Points represent outliers. P-value: two-sided Wilcoxon rank-sum test (***, $p \leq 0.001$; NS., $p>0.05$).


a
E11.5
pearson Correlation
1
0.9
0.8
0.7
0.6
PA2_Wt_1
PA2_Wt_2
Md_Wt_2
Md_Wt_1
FNP_Wt_2
Mx_Wt_1
FNP_Wt_1
Mx_Wt_2
PA2_Ezh2cKO_2
Mx_Ezh2cKO_1
FNP_Ezh2cKO_1
FNP_Ezh2cKO_2
Mx_Ezh2cKO_2
PA2_Ezh2cKO_1
Md_Ezh2cKO_1
Md_Ezh2cKO_2
b
WT, E11.5
Ezh2cKO, E11.5
Mx
FNP
Md
PA2
value
400
300
200
100
0
c.
Delta Euclidean distance
60
40
20
0
WT
Ezh2cKO
d
PCA of RNA-seq data (E11.5)
PC2, 18.55% variation
PC1, 25.77% variation
FNP_Ezh2cKO_2
FNP_Ezh2cKO_3
FNP_Ezh2cKO_1
Mx_Ezh2cKO_1
Mx_Ezh2cKO_2
Mx_Ezh2cKO_3
Md_Ezh2cKO_3
Md_Ezh2cKO_1
PA2_Ezh2cKO_2
Md_Ezh2cKO_2
PA2_Ezh2cKO_3
PA2_Ezh2cKO_1
FNP_WT_1
FNP_WT_3
FNP_WT_2
Mx_WT_2
Mx_WT_3
Mx_WT_1
Md_WT_2
Md_WT_3
Md_WT_1
PA2_WT_2
PA2_WT_3
PA2_WT_1
e
E8.5 WT
Pc−marked P−P
Pc−marked Hox−Hox
FNP E11.5 WT
FNP E11.5 Ezh2cKO
Md E11.5 WT
Md E11.5 Ezh2cKO
Mx E11.5 WT
Mx E11.5 Ezh2cKO
PA2 E11.5 WT
PA2 E11.5 Ezh2cKO

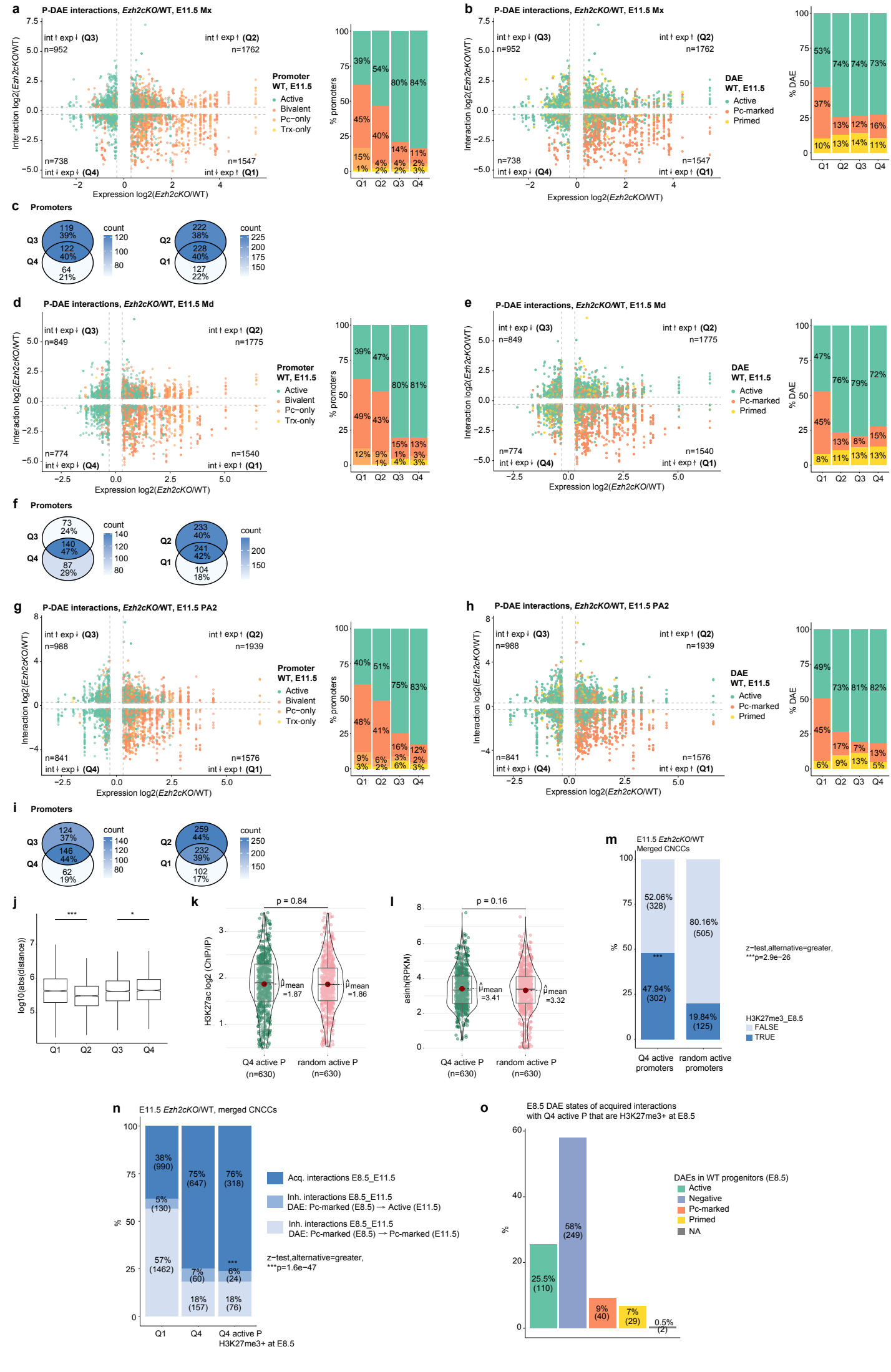
Supplementary Figure 14: Impact of Ezh2 deletion on transcriptional and chromatin structure specificities of the distinct cranial neural crest cell subpopulations

(**a**) Hierarchically clustered pairwise Pearson's correlation plot for Promoter Capture Hi-C (PCHi-C) assay values from E11.5 WT and *Ezh2cKO* cranial neural crest cell (CNCC) subpopulations (frontonasal (FNP), maxillary (Mx), mandibular (Md) and second pharyngeal arch (PA2)), with n=2 biological replicates per sample. (**b**, **c**) Euclidean distance analysis of the post-migratory CNCC subpopulations (FNP, Mx, Md and PA2) between WT and *Ezh2cKO* conditions, using PCHi-C data; visualized as heatmaps (**b**) and boxplots of the delta Euclidean distance (**c**). The results indicate that *Ezh2cKO* post-migratory CNCC subpopulations lose their chromatin structure specificities. (**d**) Principal component analysis (PCA) plot of RNA-seq data from WT and *Ezh2cKO* CNCC subpopulations (FNP, Mx, Md and PA2) at E11.5; n=3 biological replicates per sample. (**e**) Circus plots showing Pc-marked Promoter-Promoter (P-P) interactions (grey lines) and Pc-marked P-P interactions from Hox clusters (red lines) in E8.5 WT pre-migratory progenitors and in each E11.5 post-migratory WT and *Ezh2cKO* CNCC subpopulation (FNP, Mx, Md and PA2). The plot highlights the loss of Pc-marked P-P interactions, particularly inter-chromosomal interactions involving Hox clusters.


a
E11.5 FNP Ezh2cKO vs. WT
Inter-TAD 49.91%
Intra-TAD 50.09%
Inter-TAD 35.53%
Intra-TAD 64.47%
b
E11.5 Mx Ezh2cKO vs. WT
Inter-TAD 51.8%
Intra-TAD 48.2%
Inter-TAD 36.36%
Intra-TAD 63.64%
c
E11.5 Md Ezh2cKO vs. WT
Inter-TAD 22.67%
Intra-TAD 77.33%
Inter-TAD 9.14%
Intra-TAD 90.86%
d
E11.5 PA2 Ezh2cKO vs. WT
Inter-TAD 36.84%
Intra-TAD 63.16%
Inter-TAD 19.56%
Intra-TAD 80.44%
−log10(weighted_pvalue)
log2FoldChange
Intra-TAD
Inter-TAD
NA
e
E11.5, Md
***
TAD Strength
WT
Ezh2cKO
f
n=2609
E11.5, Md
Log2 Ezh2cKO/WT
TADs
g
E11.5, Md
WT
Ezh2cKO
pixels
Max Agg
h
CTCF binding, Ezh2cKO vs. WT, E11.5
log2 CTCF Ezh2cKO
log2 CTCF WT
H3K27me3 WT

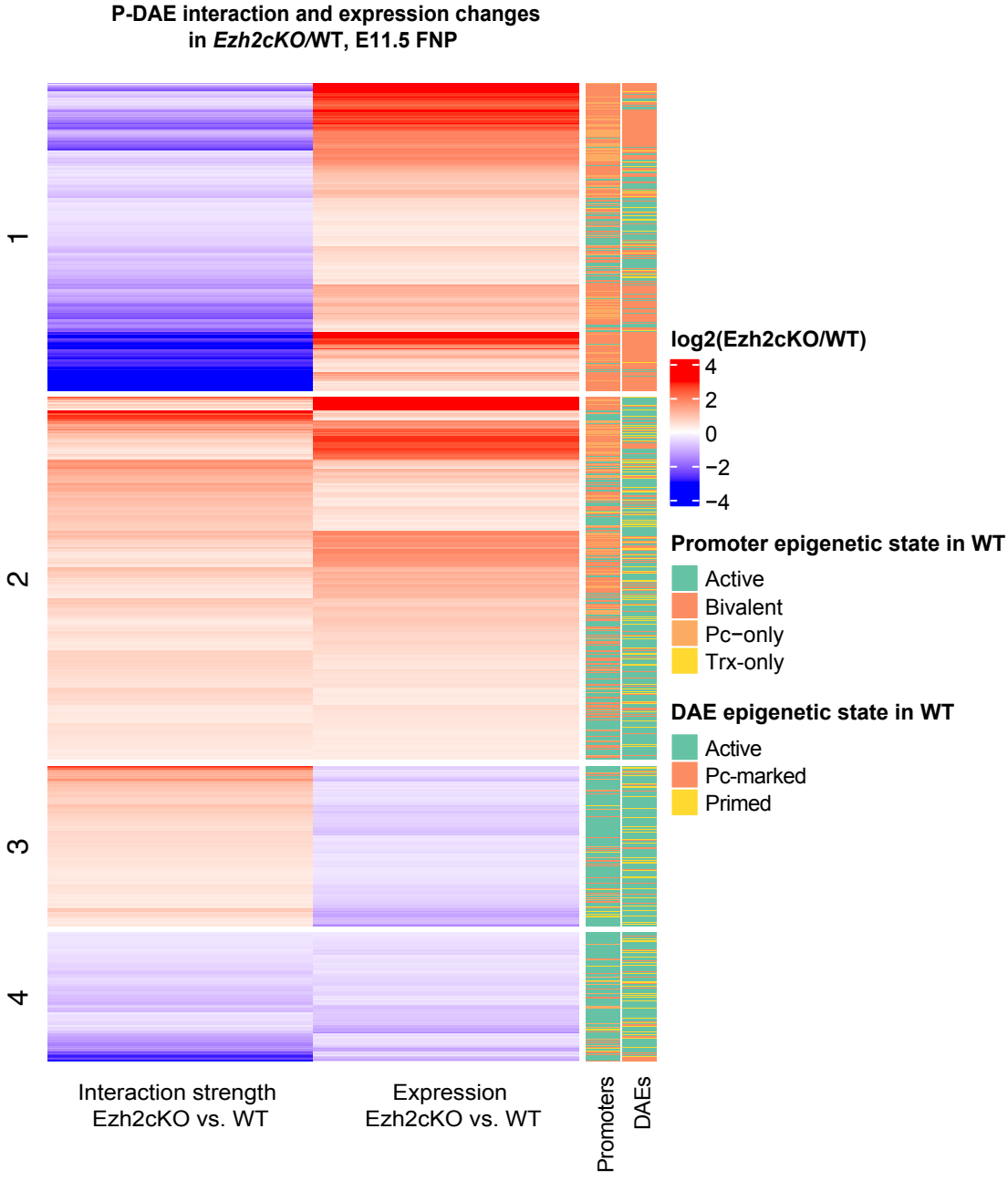
Supplementary Figure 15: Differential chromatin interactions, CTCF binding and TAD strength between *Ezh2cKO* and WT cranial neural crest cells.

(**a**-**d**) Volcano plots of differential Promoter-Distal Accessible Element (P-DAE) interactions between E11.5 *Ezh2cKO* and WT cranial neural crest cell (CNCC) subpopulations: frontonasal (FNP) (**a**), maxillary (Mx) (**b**), mandibular (Md) (**c**) and second pharyngeal arch (PA2) (**d**). Points represent interactions, color-code based on whether they are intra-TAD or inter-TAD. Significant interactions (weighted p-value ≤ 0.05, |LogFC|≥1 are indicated by dashed grey lines. Percentages indicate the proportion of interactions in each category. (**e**) Boxplot of TAD strength (log2 observed/expected) in E11.5 WT and *Ezh2cKO* Md CNCCs, calculated from Hi-C matrices at 100 kb resolution (n=2609 TADs identified from Hi-C matrices of combined E10.5 WT FNP/Mx/Md CNCCs). Box plots indicate median (middle line), interquartile range (IQR; box) and whiskers extending to 1.5×IQR. Points represent outliers; red dots indicate the mean. P-value: two-sided Wilcoxon rank-sum test (***, p ≤ 0.001). (**f**) Heatmap displaying the log2(*Ezh2cKO*/WT) ratio from aggregate TAD analysis of WT and *Ezh2cKO* Md Hi-C datasets at 100 kb resolution, using the TADs (n=2609) identified in (**e**). This heatmap provides an average Hi-C matrix view of TAD structures in both conditions, revealing differences in TAD organization between WT and *Ezh2cKO*. (**g**) Line plot from (**f**) showing the maximum aggregate values (log2 observed/expected) per pixel for WT vs. *Ezh2cKO* Md, highlighting the presence of stronger TAD borders in *Ezh2cKO*. (**h**) Scatter plot of CTCF binding sites, comparing E11.5 WT (x axis) and E11.5 *Ezh2cKO* (y axis) FNP, Mx, Md and PA2 merged prominences. Color code represents H3K27me3 enrichment in WT CNCCs.


a
P-DAE interactions, Ezh2cKO/WT, E11.5 Mx
int↑ exp↑ (Q3) n=952
int↑ exp↑ (Q2) n=1762
int↓ exp↓ (Q4) n=738
int↓ exp↑ (Q1) n=1547
Interaction log2(Ezh2cKO/WT)
Expression log2(Ezh2cKO/WT)
Promoter WT, E11.5
Active
Bivalent
Pc−only
Trx−only
% promoters
39% 54% 80% 84%
45% 40% 14% 11%
15% 4% 4% 3%
1% 2% 2%
Q1 Q2 Q3 Q4
b
P-DAE interactions, Ezh2cKO/WT, E11.5 Mx
DAE WT, E11.5
Active
Pc-marked
Primed
% DAE
53% 74% 74% 73%
37% 13% 12% 16%
10% 13% 14% 11%
c
Promoters
Q3 Q4 Q2 Q1
count
119 39%
122 40%
64 21%
222 38%
228 40%
127 22%
d
P-DAE interactions, Ezh2cKO/WT, E11.5 Md
n=849
n=1775
n=774
n=1540
39% 47% 80% 81%
49% 43% 15% 13%
12% 9% 1% 3%
1% 4% 3%
e
P-DAE interactions, Ezh2cKO/WT, E11.5 Md
47% 76% 79% 72%
45% 13% 8% 15%
8% 11% 13% 13%
f
Promoters
73 24%
140 47%
87 29%
233 40%
241 42%
104 18%
g
P-DAE interactions, Ezh2cKO/WT, E11.5 PA2
n=988
n=1939
n=841
n=1576
40% 51% 75% 83%
48% 41% 16% 12%
9% 6% 3% 2%
3% 2% 6% 3%
h
P-DAE interactions, Ezh2cKO/WT, E11.5 PA2
49% 73% 81% 82%
45% 17% 7% 13%
6% 9% 13% 5%
i
Promoters
124 37%
146 44%
62 19%
259 44%
232 39%
102 17%
j
log10(abs(distance))
***
*
k
p = 0.84
H3K27ac log2 (ChIP/IP)
μ̂mean =1.87
μ̂mean =1.86
Q4 active P (n=630)
random active P (n=630)
l
p = 0.16
asinh(RPKM)
μ̂mean =3.41
μ̂mean =3.32
m
E11.5 Ezh2cKO/WT Merged CNCCs
52.06% (328)
80.16% (505)
***
47.94% (302)
19.84% (125)
Q4 active promoters
random active promoters
z−test,alternative=greater, ***p=2.9e−26
H3K27me3_E8.5
FALSE
TRUE
n
E11.5 Ezh2cKO/WT, merged CNCCs
38% (990)
75% (647)
76% (318)
5% (130)
57% (1462)
7% (60)
6% (24)
18% (157)
18% (76)
Q1
Q4
Q4 active P H3K27me3+ at E8.5
Acq. interactions E8.5_E11.5
Inh. interactions E8.5_E11.5 DAE: Pc-marked (E8.5) → Active (E11.5)
Inh. interactions E8.5_E11.5 DAE: Pc-marked (E8.5) → Pc-marked (E11.5)
z−test,alternative=greater, ***p=1.6e−47
o
E8.5 DAE states of acquired interactions with Q4 active P that are H3K27me3+ at E8.5
25.5% (110)
58% (249)
9% (40)
7% (29)
0.5% (2)
DAEs in WT progenitors (E8.5)
Active
Negative
Pc-marked
Primed
NA

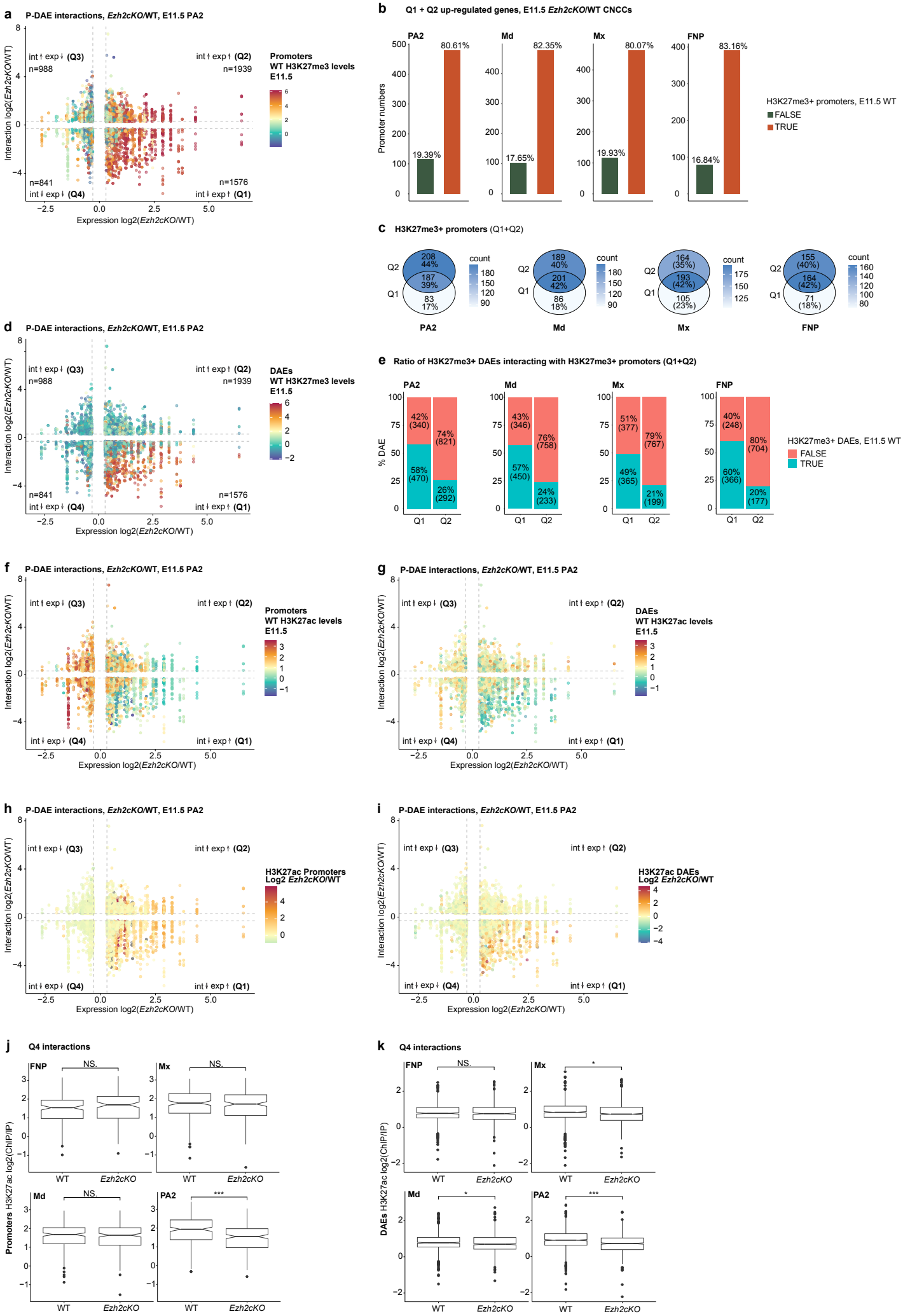
Supplementary Figure 16: Epigenetic and 3D chromatin landscape of promoter-DAE interactions in *Ezh2cKO* vs. WT cranial neural crest cells

(**a**-**b**) Scatter plots of Promoter-Distal Accessible Element (P-DAE) interactions in E11.5 maxillary (Mx) CNCCs, comparing *Ezh2cKO* and WT. The x-axis shows log2 fold change (log2FC) in target gene expression and the y-axis log2FC in interaction strength. Each point represents one interaction, with matched positions across plots and colored according to the epigenetic states of promoters (**a**) or DAEs (**b**) in E11.5 WT Mx CNCCs. Negative promoters and DAEs were excluded. Adjacent bar plots show the proportion of promoters (**a**) or DAEs (**b**) from each epigenetic class within the four quadrants (Q1-Q4) defined by |log2 FC|≥0.3 on both axes (dashed grey lines). (**c**) Venn diagram showing the overlap between unique promoters involved in Q3 + Q4 interactions and in Q1 + Q2 interactions, from (**a**). (**d**-**f**) and (**g**-**i**) Same analysis as in (**a**-**c**) for E11.5 mandibular (Md) (**d**-**f**) and second pharyngeal arch (PA2) (**g**-**i**) CNCC subpopulations. (**j**) Box plot showing the log10 distance distribution of interactions across quadrants (Q1-Q4), with data merged from all E11.5 CNCC subpopulations (FNP, Mx, Md and PA2). P-value: two-sided Wilcoxon rank-sum test (*, p ≤0.05; ***, p ≤ 0.001). (**k**, **l**) Violin plots showing H3K27ac enrichment (**k**) and target gene expression levels (**l**) of Q4 active promoters across all E11.5 WT CNCC subpopulations, compared with a random set of active promoters matched for H3K27ac and expression. P-value: two-sided Welch's t-test. In **j**, **k** and **l**, box plots indicate median (middle line), interquartile range (IQR; box) and whiskers extending to 1.5×IQR. In **k** and **l**, all data points are shown; red dots indicate the mean. (**m**) Bar plot showing the percentage of E11.5 Q4 active promoters that carried H3K27me3 in E8.5 WT progenitors, compared with the matched random set described in (**k**, **l**). 48% of Q4 active promoters were H3K27me3+ in progenitors, compared to only 20% in the random set (***, p ≤ 0.001, one-sided Z-test). (**n**) Bar plot showing the percentages of acquired (Acq.) and inherited (Inh.) interactions (int) from E8.5 to E11.5, at E11.5 Q1 promoters, Q4 promoters, and Q4 active promoters that were H3K27me3+ in progenitors. Inherited interactions are subdivided into those involving Pc-marked DAEs at E8.5 that have switched to active at E11.5 (poised enhancers), and those involving DAEs that remain Pc-marked. Acquired interactions are significantly enriched at Q4 promoters and at Q4 active promoters previously H3K27me3+ in progenitors (***, p ≤ 0.001, one-sided Z-test). (**o**) Bar plot showing the epigenetic states at E8.5 of the DAEs that acquire interactions with E11.5 Q4 active promoters previously H3K27me3+ in progenitors. Most DAEs were negative or already active at E8.5.


P-DAE interaction and expression changes
in Ezh2cKO/WT, E11.5 FNP
1
2
3
4
Interaction strength
Ezh2cKO vs. WT
Expression
Ezh2cKO vs. WT
Promoters
DAEs
log2(Ezh2cKO/WT)
4
2
0
−2
−4
Promoter epigenetic state in WT
Active
Bivalent
Pc−only
Trx-only
DAE epigenetic state in WT
Active
Pc-marked
Primed

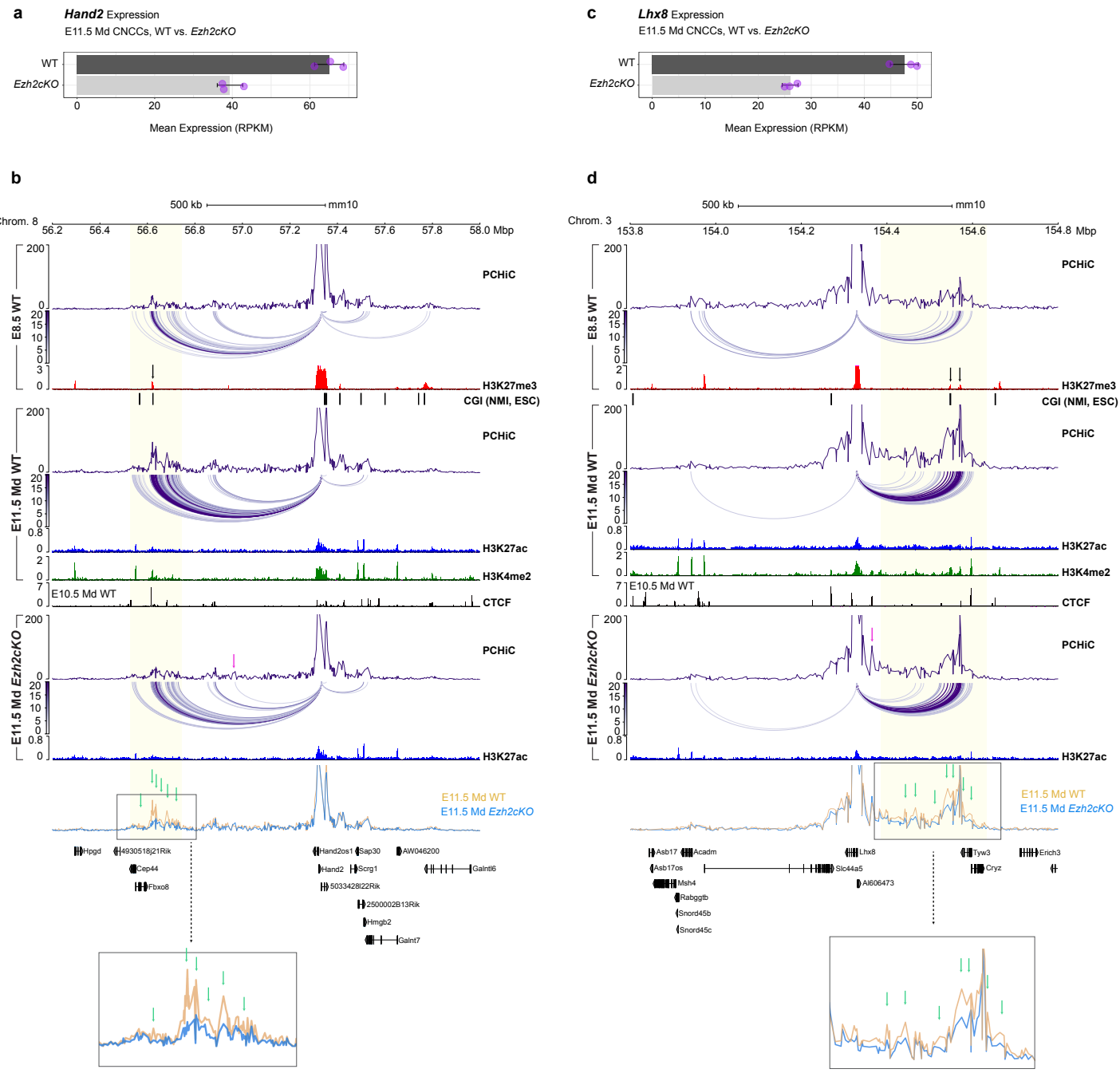
Supplementary Figure 17: Heat map summarizing the relationship between chromatin interaction strength and gene expression changes in E11.5 *Ezh2cKO* versus WT frontonasal cranial neural crest cells (CNCCs).

Promoter–distal accessible element (DAE) pairs were clustered into four groups corresponding to the four quadrants (Q1-Q4) defined by |log2 FC|≥0.3 on both axes (dashed grey lines) in the scatter plot presented Fig. 5b, representing distinct combinations of interaction and expression changes. The heat map displays log2 fold changes in interaction strength and gene expression (Ezh2cKO vs. WT) in E11.5 frontonasal (FNP) CNCCs, together with the epigenetic state of promoters and associated DAEs in E11.5 WT FNP CNCCs.


a
P-DAE interactions, Ezh2cKO/WT, E11.5 PA2
int↑ exp↓ (Q3)
n=988
int↑ exp↑ (Q2)
n=1939
n=841
int↓ exp↓ (Q4)
n=1576
int↓ exp↑ (Q1)
Interaction log2(Ezh2cKO/WT)
Expression log2(Ezh2cKO/WT)
Promoters
WT H3K27me3 levels
E11.5
b
Q1 + Q2 up-regulated genes, E11.5 Ezh2cKO/WT CNCCs
PA2
Md
Mx
FNP
Promoter numbers
80.61%
19.39%
82.35%
17.65%
80.07%
19.93%
83.16%
16.84%
H3K27me3+ promoters, E11.5 WT
FALSE
TRUE
c
H3K27me3+ promoters (Q1+Q2)
Q2
Q1
208
44%
187
39%
83
17%
189
40%
201
42%
86
18%
164
(35%)
193
(42%)
105
(23%)
155
(40%)
164
(42%)
71
(18%)
count
d
P-DAE interactions, Ezh2cKO/WT, E11.5 PA2
DAEs
WT H3K27me3 levels
E11.5
e
Ratio of H3K27me3+ DAEs interacting with H3K27me3+ promoters (Q1+Q2)
% DAE
42%
(340)
58%
(470)
74%
(821)
26%
(292)
43%
(346)
57%
(450)
76%
(758)
24%
(233)
51%
(377)
49%
(365)
79%
(767)
21%
(199)
40%
(248)
60%
(366)
80%
(704)
20%
(177)
H3K27me3+ DAEs, E11.5 WT
FALSE
TRUE
f
P-DAE interactions, Ezh2cKO/WT, E11.5 PA2
Promoters
WT H3K27ac levels
E11.5
g
P-DAE interactions, Ezh2cKO/WT, E11.5 PA2
DAEs
WT H3K27ac levels
E11.5
h
P-DAE interactions, Ezh2cKO/WT, E11.5 PA2
H3K27ac Promoters
Log2 Ezh2cKO/WT
i
P-DAE interactions, Ezh2cKO/WT, E11.5 PA2
H3K27ac DAEs
Log2 Ezh2cKO/WT
j
Q4 interactions
FNP
Mx
Md
PA2
NS.
***
WT
Ezh2cKO
Promoters H3K27ac log2(ChIP/IP)
k
Q4 interactions
FNP
Mx
Md
PA2
NS.
*
***
WT
Ezh2cKO
DAEs H3K27ac log2(ChIP/IP)

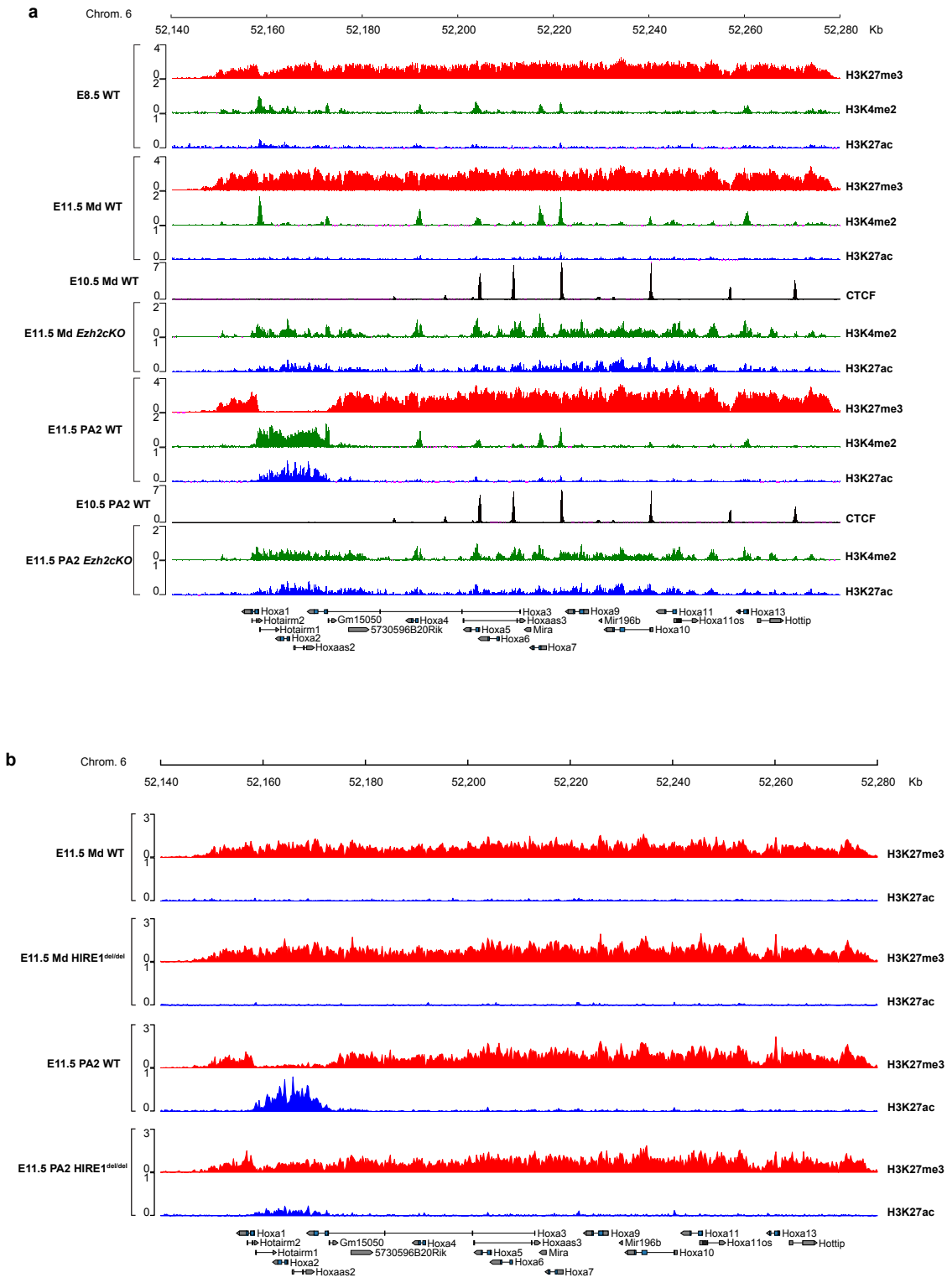
Supplementary Figure 18: Epigenetic characterization of interactions involved in transcriptional down- and up-regulation in *Ezh2cKO* cranial neural crest cells

(**a**) Scatter plot of Promoter-Distal Accessible Element (P-DAE) interactions in E11.5 second pharyngeal arch (PA2) cranial neural crest cells (CNCCs), comparing *Ezh2cKO* and WT. The x-axis shows the log2 fold change (log2FC) in target gene expression and the y-axis shows the log2FC in interaction strength. Each point represents one P-DAE interaction and is color-coded based on the H3K27me3 levels of the promoters in WT PA2 at E11.5. (**b**) Bar plots showing the percentage of H3K27me3-positive promoters (in E11.5 WT CNCCs) among genes upregulated in *Ezh2cKO* vs. WT CNCCs, considering only those that simultaneously exhibit changes in 3D chromatin conformation (Q1+Q2 promoters). Percentages are shown for each CNCC subpopulation. (**c**) Venn diagrams showing the overlap of unique H3K27me3-positive promoters (in E11.5 WT CNCCs) involved in Q1 + Q2 interactions across E11.5 CNCC subpopulations. (**d**) Scatter plot as in (**a**), but with color-coding based on the H3K27me3 levels of the DAEs in WT PA2 at E11.5. (**e**) Bar plots showing the ratio of H3K27me3-positive DAEs interacting with Q1+Q2 H3K27me3-positive promoters, for each E11.5 CNCC subpopulation. (**f**-**g**) Scatter plots as in (**a**), but with color-coding based on the H3K27ac levels of the promoters (**f**) and DAEs (**g**) in WT PA2 at E11.5. (**h**-**i**) Scatter plots as in (**a**), but with color-coding based on the $\log_2$ fold change in H3K27ac levels between *Ezh2cKO* and WT CNCCs, measured at the promoters (**h**) and DAEs (**i**). (**j**-**k)** Box plots showing H3K27ac levels at promoters (**j**) and DAEs (**k**) involved in Q4 interactions, comparing WT and *Ezh2cKO* CNCCs. Each CNCC subpopulation is shown. Box plots indicate median (middle line), interquartile range (IQR; box) and whiskers extending to 1.5×IQR. Points represent outliers. P-value: two-sided Wilcoxon rank-sum test (***, $p \leq 0.001$; **, $p \leq 0.01$; *, $p < 0.05$, NS., $p > 0.05$).

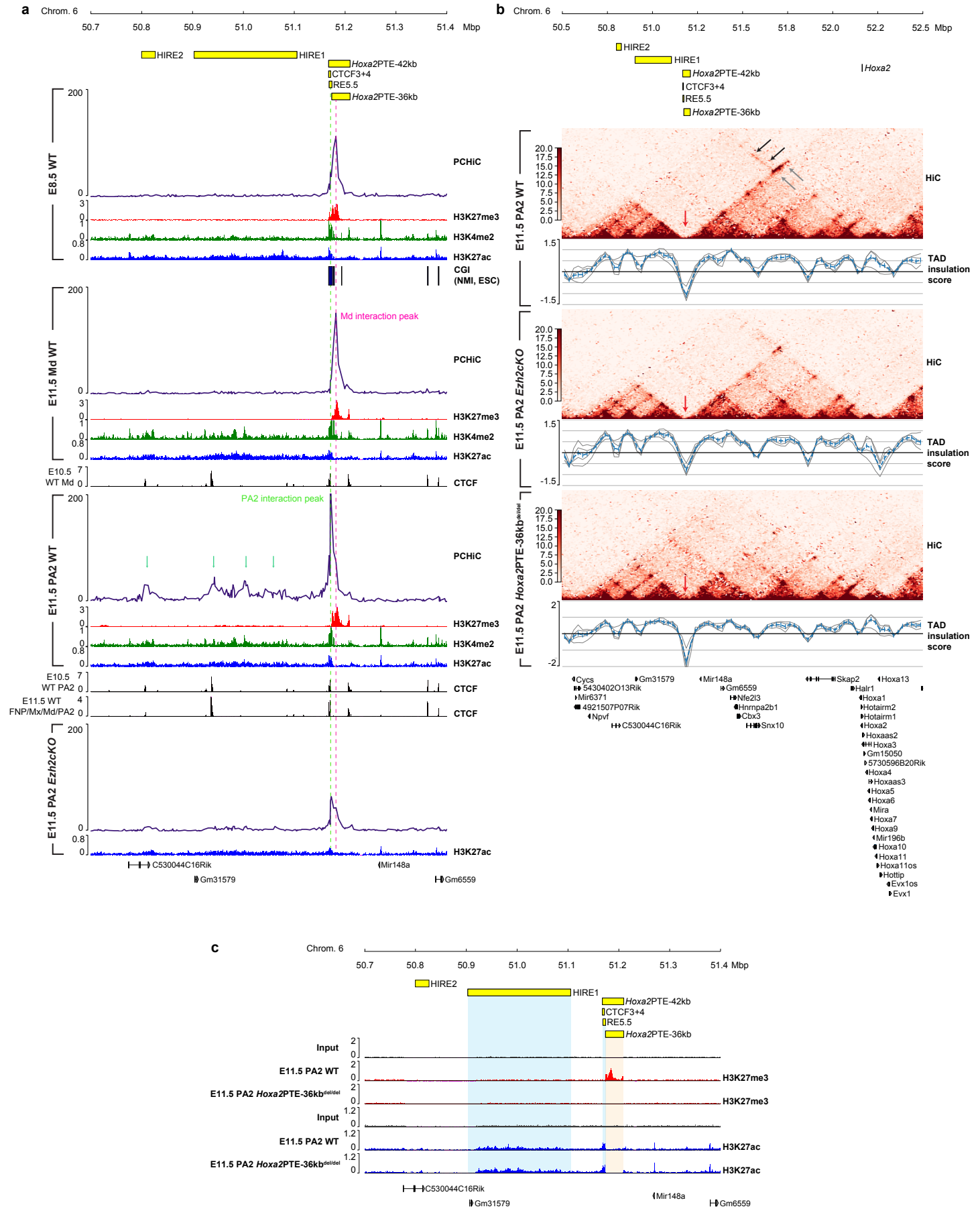

a
Hand2 Expression
E11.5 Md CNCCs, WT vs. Ezh2cKO
WT
Ezh2cKO
0
20
40
60
Mean Expression (RPKM)
c
Lhx8 Expression
E11.5 Md CNCCs, WT vs. Ezh2cKO
WT
Ezh2cKO
0
10
20
30
40
50
Mean Expression (RPKM)
b
500 kb
mm10
Chrom. 8
56.2
56.4
56.6
56.8
57.0
57.2
57.4
57.6
57.8
58.0 Mbp
E8.5 WT
PCHiC
H3K27me3
CGI (NMI, ESC)
E11.5 Md WT
PCHiC
H3K27ac
H3K4me2
E10.5 Md WT
CTCF
E11.5 Md Ezh2cKO
PCHiC
H3K27ac
E11.5 Md WT
E11.5 Md Ezh2cKO
Hpgd
4930518j21Rik
Cep44
Fbxo8
Hand2os1
Sap30
AW046200
Hand2
Scrg1
Galntl6
5033428I22Rik
2500002B13Rik
Hmgb2
Galnt7
d
500 kb
mm10
Chrom. 3
153.8
154.0
154.2
154.4
154.6
154.8 Mbp
E8.5 WT
PCHiC
H3K27me3
CGI (NMI, ESC)
E11.5 Md WT
PCHiC
H3K27ac
H3K4me2
E10.5 Md WT
CTCF
E11.5 Md Ezh2cKO
PCHiC
H3K27ac
E11.5 Md WT
E11.5 Md Ezh2cKO
Asb17
Acadm
Asb17os
Msh4
Rabggtb
Snord45b
Snord45c
Lhx8
Slc44a5
AI606473
Tyw3
Cryz
Erich3

Supplementary Figure 19: Impact of Ezh2 deletion on *Hand2* and *Lhx8* expression and chromatin interactions in the mandibular process

(**a**) Bar plot showing *Hand2* expression levels (RPKM) in E11.5 WT and *Ezh2cKO* mandibular (Md) CNCCs. n= 3 biological replicates per genotype. Data are presented as mean values +/- SD. (**b**) Genome browser view of chromosome 8 (56,200,000–58,000,000) showing significant *Hand2* PCHi-C interactions (CHiCAGO score ≥ 5, purple arcs) and cis-interaction profile (purple lines) in E8.5 WT progenitors; E11.5 Md WT CNCCs and E11.5 Md *Ezh2cKO* CNCCs. CpG island (CGI) enrichment is from ES cells (NMI dataset[53]). ChIP-seq tracks show H3K27me3 (red) in E8.5 WT progenitors, H3K27ac (blue) in E11.5 Md WT and *Ezh2cKO* CNCCs, H3K4me2 (green) in E11.5 Md WT CNCCs and CTCF (black) in E10.5 WT Md. The black arrow indicates a putative PTE interacting with the *Hand2* promoter in progenitors. At the bottom, a superposition of the *Hand2* cis-interaction profiles from E11.5 Md *Ezh2cKO* CNCCs (blue line) and E11.5 Md WT CNCCs (orange line) is shown. Green arrows indicate reduced interactions between *Hand2* and its enhancer region in E11.5 Md *Ezh2cKO* CNCCs compared with WT. The pink arrow highlights the gain of ectopic short-range interactions in E11.5 Md *Ezh2cKO* CNCCs. (**c**) Bar plot showing *Lhx8* expression levels (RPKM) in E11.5 WT and *Ezh2cKO* Md CNCCs. n= 3 biological replicates per genotype. Data are presented as mean values +/- SD. (**d**) Genome browser view of chromosome 3 (153,800,000–154,800,000) showing significant *Lhx8* PCHi-C interactions (CHiCAGO score ≥ 5, purple arcs) and cis-interaction profile (purple lines) in E8.5 WT progenitors; E11.5 Md WT CNCCs and E11.5 Md *Ezh2cKO* CNCCs. CpG island (CGI) enrichment is from ES cells (NMI dataset[53]). ChIP-seq tracks show H3K27me3 (red) in E8.5 WT progenitors, H3K27ac (blue) in E11.5 Md WT and *Ezh2cKO* CNCCs, H3K4me2 (green) in E11.5 Md WT CNCCs and CTCF (black) in E10.5 WT Md. The black arrows indicate putative PTEs interacting with the *Lhx8* promoter in progenitors. At the bottom, a superposition of the *Lhx8* cis-interaction profiles from E11.5 Md *Ezh2cKO* CNCCs (blue line) and E11.5 Md WT CNCCs (orange line) is shown. Green arrows indicate reduced interactions between *Lhx8* and its enhancer region in E11.5 Md *Ezh2cKO* CNCCs compared with WT. The pink arrow highlights the gain of ectopic short-range interactions in E11.5 Md *Ezh2cKO* CNCCs.

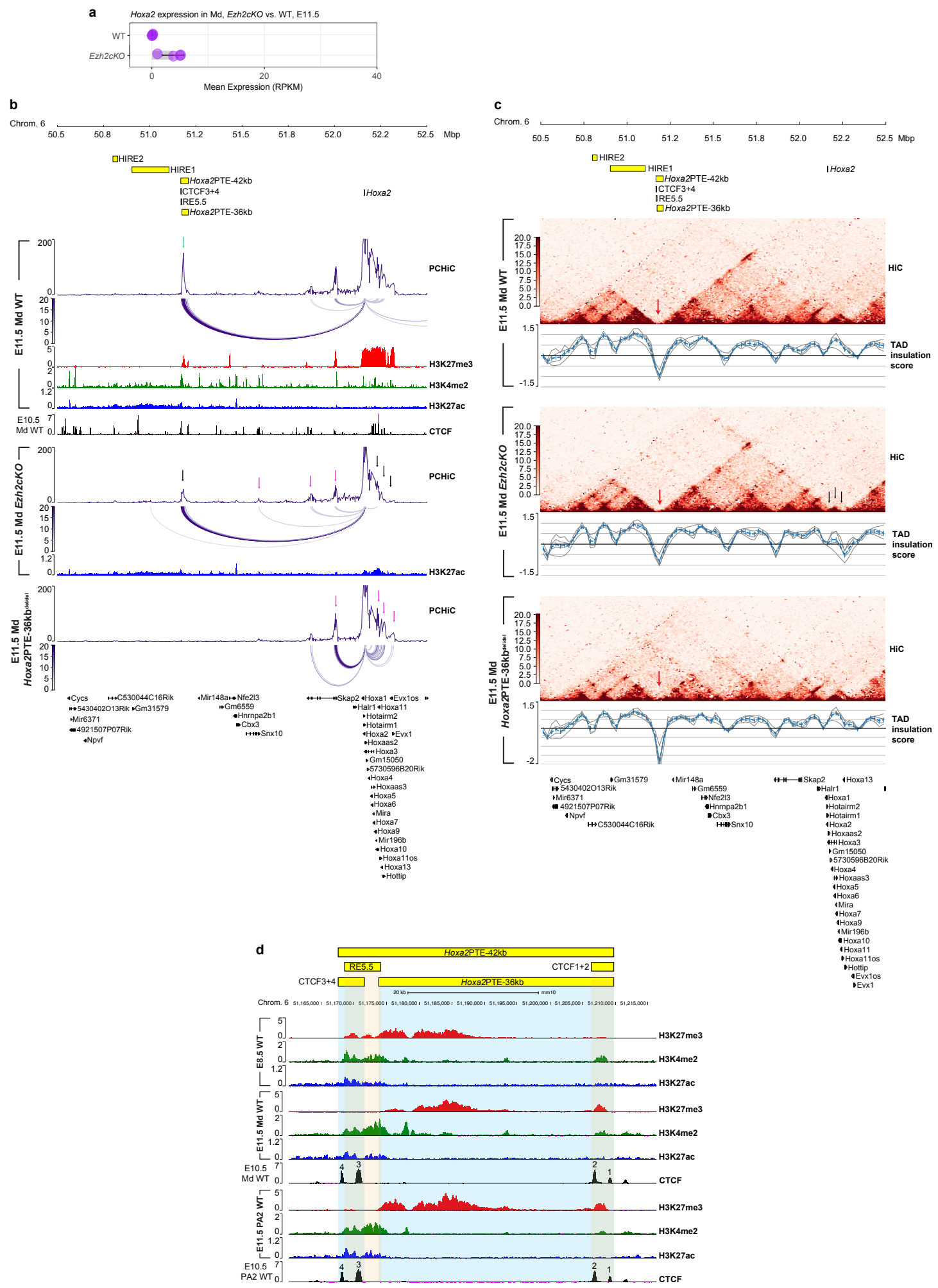

a
Chrom. 6
52,140
52,160
52,180
52,200
52,220
52,240
52,260
52,280
Kb
E8.5 WT
H3K27me3
H3K4me2
H3K27ac
E11.5 Md WT
H3K27me3
H3K4me2
H3K27ac
E10.5 Md WT
CTCF
E11.5 Md Ezh2cKO
H3K4me2
H3K27ac
E11.5 PA2 WT
H3K27me3
H3K4me2
H3K27ac
E10.5 PA2 WT
CTCF
E11.5 PA2 Ezh2cKO
H3K4me2
H3K27ac
Hoxa1
Hotairm2
Hotairm1
Hoxa2
Hoxaas2
Gm15050
5730596B20Rik
Hoxa4
Hoxa3
Hoxaas3
Hoxa5
Mira
Hoxa6
Hoxa7
Hoxa9
Mir196b
Hoxa10
Hoxa11
Hoxa11os
Hoxa13
Hottip
b
Chrom. 6
52,140
52,160
52,180
52,200
52,220
52,240
52,260
52,280
Kb
E11.5 Md WT
H3K27me3
H3K27ac
E11.5 Md HIRE1del/del
H3K27me3
H3K27ac
E11.5 PA2 WT
H3K27me3
H3K27ac
E11.5 PA2 HIRE1del/del
H3K27me3
H3K27ac
Hoxa1
Hotairm2
Hotairm1
Hoxa2
Hoxaas2
Gm15050
5730596B20Rik
Hoxa4
Hoxa3
Hoxaas3
Hoxa5
Mira
Hoxa6
Hoxa7
Hoxa9
Mir196b
Hoxa10
Hoxa11
Hoxa11os
Hoxa13
Hottip

Supplementary Figure 20: Effects of HIRE1 deletion on chromatin state at the *Hoxa* locus. (**a**) *Hoxa* cluster genome browser view with ChIP-seq profiles for H3K27me3 (red), H3K4me2 (green) and H3K27ac (blue) in E8.5 WT pre-migratory progenitors, and E11.5 WT and *Ezh2cKO* mandibular (Md) and second pharyngeal arch (PA2) cranial neural crest cells (CNCCs). The CTCF ChIP-seq profiles (black) in E10.5 WT Md and PA2 are also shown. (**b**) *Hoxa* cluster genome browser view with ChIP-seq profiles for H3K27me3 (red) and H3K27ac (blue) from the mandibular process (Md) and the second pharyngeal arch (PA2) of E11.5 WT and *HIRE1*$^{del/del}$ embryos.


a
Chrom. 6
50.7 50.8 50.9 51.0 51.1 51.2 51.3 51.4 Mbp
HIRE2
HIRE1
Hoxa2PTE-42kb
CTCF3+4
RE5.5
Hoxa2PTE-36kb
E8.5 WT
PCHiC
H3K27me3
H3K4me2
H3K27ac
CGI (NMI, ESC)
E11.5 Md WT
Md interaction peak
PCHiC
H3K27me3
H3K4me2
H3K27ac
E10.5 WT Md
CTCF
E11.5 PA2 WT
PA2 interaction peak
PCHiC
H3K27me3
H3K4me2
H3K27ac
E10.5 WT PA2
CTCF
E11.5 WT FNP/Mx/Md/PA2
CTCF
E11.5 PA2 Ezh2cKO
H3K27ac
C530044C16Rik
Mir148a
Gm31579
Gm6559
b
Chrom. 6
50.5 50.8 51.0 51.2 51.5 51.8 52.0 52.2 52.5 Mbp
HIRE2
HIRE1
Hoxa2PTE-42kb
CTCF3+4
RE5.5
Hoxa2PTE-36kb
Hoxa2
E11.5 PA2 WT
HiC
TAD insulation score
E11.5 PA2 Ezh2cKO
HiC
TAD insulation score
E11.5 PA2 Hoxa2PTE-36kbdel/del
HiC
TAD insulation score
Cycs
5430402O13Rik
Mir6371
4921507P07Rik
Npvf
Gm31579
C530044C16Rik
Mir148a
Gm6559
Nfe2l3
Hnrnpa2b1
Cbx3
Snx10
Skap2
Hoxa13
Halr1
Hoxa1
Hotairm2
Hotairm1
Hoxa2
Hoxaas2
Hoxa3
Gm15050
5730596B20Rik
Hoxa4
Hoxaas3
Hoxa5
Hoxa6
Mira
Hoxa7
Hoxa9
Mir196b
Hoxa10
Hoxa11
Hoxa11os
Hottip
Evx1os
Evx1
c
Chrom. 6
50.7 50.8 50.9 51.0 51.1 51.2 51.3 51.4 Mbp
HIRE2
HIRE1
Hoxa2PTE-42kb
CTCF3+4
RE5.5
Hoxa2PTE-36kb
Input
E11.5 PA2 WT
H3K27me3
E11.5 PA2 Hoxa2PTE-36kbdel/del
H3K27me3
Input
E11.5 PA2 WT
H3K27ac
E11.5 PA2 Hoxa2PTE-36kbdel/del
H3K27ac
C530044C16Rik
Mir148a
Gm31579
Gm6559

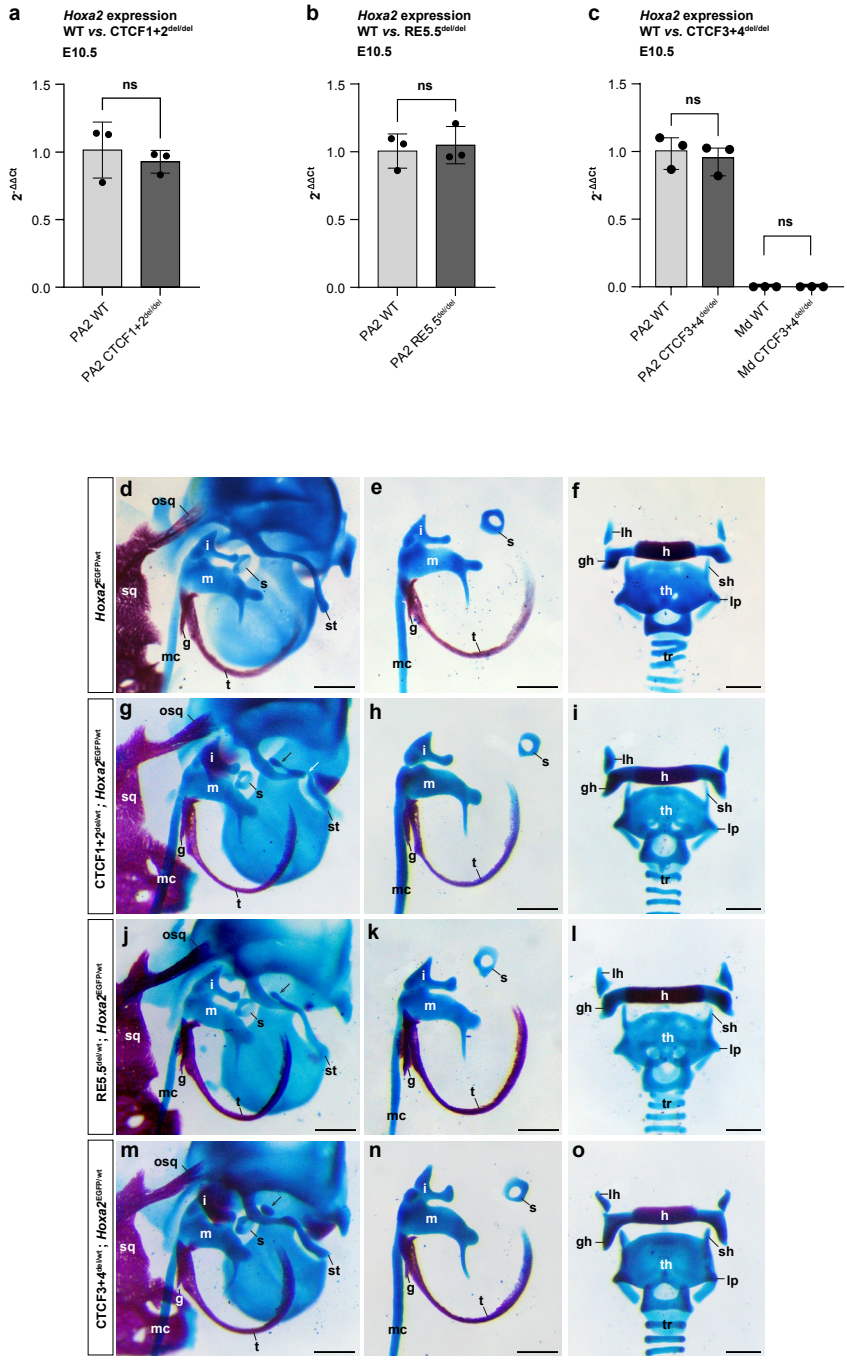
Supplementary Figure 21: Impact of Ezh2 and *Hoxa2*PTE-36kb deletions on the epigenetic and chromatin interaction landscapes of *Hoxa2*

(**a**) Genome browser view of a zoomed-in region from Fig. 6, focusing on the *Hoxa2*PTE-36kb and HIRE1/HIRE2 super-enhancer regions. The cis-interaction profile of *Hoxa2* (purple lines) is shown for E8.5 WT pre-migratory progenitors, E11.5 mandibular (Md) and second pharyngeal arch (PA2) WT CNCCs, and E11.5 PA2 *Ezh2cKO* CNCCs. Green arrows indicate *Hoxa2* interactions with HIRE1/HIRE2 in E11.5 PA2 WT CNCCs. CpG island (CGI) enrichment is from ES cells (NMI dataset[53]). ChIP-seq tracks show H3K27me3 (red), H3K4me2 (green) and H3K27ac (blue) in E8.5 WT progenitors and E11.5 Md and PA2 WT CNCCs; CTCF (black) in E10.5 WT Md and PA2 and in merged E11.5 WT FNP/Mx/Md/PA2 prominences; H3K27ac (blue) in E11.5 PA2 *Ezh2cKO* CNCCs. The dashed blue line represents TAD insulation scores derived from mixed E10.5 FNP, Mx and Md WT CNCCs. Grey lines represent calculation with different window sizes (Methods). The vertical dashed pink line highlights the interaction peak between the *Hoxa2* promoter and *Hoxa2*PTE-36kb in E8.5 progenitors and E11.5 Md WT CNCCs, while the vertical dashed green line highlights the interaction peak in E11.5 PA2 WT CNCCs, between the *Hoxa2* promoter and RE5.5. (**b**) Hi-C interaction heatmaps at 10kb resolution spanning a 2 Mb region of chromosome 6, containing the *Hoxa* cluster and the *Hoxa2* HIRE1/HIRE2 super-enhancer (50,500,000–52,500,000 bp) in E11.5 PA2 WT and *Ezh2cKO* CNCCs and in PA2 of *Hoxa2PTE-36kb*$^{del/del}$ mutant embryos. Insulation scores for each CNCC subpopulation are shown below. Red arrows indicate TAD border, which remain unchanged. Black arrows highlight a stripe extending across the TAD boundary, representing the interactions between the *Hoxa2* promoter and the HIRE1 super-enhancer region in E11.5 PA2 WT CNCCs, as previously reported in Kessler *et al*., 2023[24]. Grey arrows highlight interactions in E11.5 WT PA2 CNCCs, between *Hoxa2*PTE-36kb and the Pc-repressed *Hoxa* cluster genes flanking *Hoxa2*. These interactions are absent in PA2 of E11.5 *Hoxa2PTE-36kb*$^{del/del}$ mutants. (**c**) Genome browser view of the chromosome 6 (50,700,000–51,400,000) showing H3K27me3 (red) and H3K27ac (blue) ChIP-seq profiles in PA2 of E11.5 WT and *Hoxa2PTE-36kb*$^{del/del}$ embryos. In *Hoxa2PTE-36kb*$^{del/del}$ mutants, H3K27ac levels on HIRE1 and RE5.5 remain unchanged.


a
Hoxa2 expression in Md, Ezh2cKO vs. WT, E11.5
WT
Ezh2cKO
0
20
40
Mean Expression (RPKM)
b
Chrom. 6
50.5 50.8 51.0 51.2 51.5 51.8 52.0 52.2 52.5 Mbp
HIRE2
HIRE1
Hoxa2PTE-42kb
CTCF3+4
RE5.5
Hoxa2PTE-36kb
Hoxa2
E11.5 Md WT
PCHiC
H3K27me3
H3K4me2
H3K27ac
E10.5 Md WT
CTCF
E11.5 Md Ezh2cKO
PCHiC
H3K27ac
E11.5 Md Hoxa2PTE-36kbdel/del
PCHiC
Cycs
C530044C16Rik
5430402O13Rik
Gm31579
Mir6371
4921507P07Rik
Npvf
Mir148a
Nfe2l3
Gm6559
Hnrnpa2b1
Cbx3
Snx10
Skap2
Hoxa1
Evx1os
Halr1
Hoxa11
Hotairm2
Hotairm1
Hoxa2
Evx1
Hoxaas2
Hoxa3
Gm15050
5730596B20Rik
Hoxa4
Hoxaas3
Hoxa5
Hoxa6
Mira
Hoxa7
Hoxa9
Mir196b
Hoxa10
Hoxa11os
Hoxa13
Hottip
c
Chrom. 6
50.5 50.8 51.0 51.2 51.5 51.8 52.0 52.2 52.5 Mbp
HIRE2
HIRE1
Hoxa2PTE-42kb
CTCF3+4
RE5.5
Hoxa2PTE-36kb
Hoxa2
E11.5 Md WT
HiC
TAD insulation score
E11.5 Md Ezh2cKO
HiC
TAD insulation score
E11.5 Md Hoxa2PTE-36kbdel/del
HiC
TAD insulation score
Cycs
Gm31579
5430402O13Rik
Mir6371
4921507P07Rik
Npvf
C530044C16Rik
Mir148a
Gm6559
Nfe2l3
Hnrnpa2b1
Cbx3
Snx10
Skap2
Hoxa13
Halr1
Hoxa1
Hotairm2
Hotairm1
Hoxa2
Hoxaas2
Hoxa3
Gm15050
5730596B20Rik
Hoxa4
Hoxaas3
Hoxa5
Hoxa6
Mira
Hoxa7
Hoxa9
Mir196b
Hoxa10
Hoxa11
Hoxa11os
Hottip
Evx1os
Evx1
d
Hoxa2PTE-42kb
RE5.5
CTCF1+2
CTCF3+4
Hoxa2PTE-36kb
20 kb
mm10
Chrom. 6
51,165,000 51,170,000 51,175,000 51,180,000 51,185,000 51,190,000 51,195,000 51,200,000 51,205,000 51,210,000 51,215,000
E8.5 WT
H3K27me3
H3K4me2
H3K27ac
E11.5 Md WT
H3K27me3
H3K4me2
H3K27ac
E10.5 Md WT
CTCF
E11.5 PA2 WT
H3K27me3
H3K4me2
H3K27ac
E10.5 PA2 WT
CTCF

Supplementary Figure 22: Impact of Ezh2 and *Hoxa2*PTE-36kb deletions on *Hoxa2* expression and chromatin interactions in the mandibular process

(**a**) Bar plot showing *Hoxa2* expression levels (RPKM) in E11.5 WT and *Ezh2cKO* mandibular (Md) cranial neural crest cells (CNCCs). (**b**) Genome browser view showing *Hoxa2* significant promoter capture HiC (PCHi-C) interactions (CHiCAGO score ≥ 5, purple arcs) and cis-interaction profile (purple lines) in E11.5 WT and *Ezh2cKO* Md CNCCs, and in Md of E11.5 *Hoxa2PTE-36kb*$^{del/del}$ mutant embryos. ChIP-seq profiles are also shown: H3K27me3 (red), H3K4me2 (green) and H3K27ac (blue) in E11.5 Md WT CNCCs; H3K27ac (blue) in E11.5 Md *Ezh2cKO* CNCCs; CTCF (black) in E10.5 WT Md. The region spans 2 Mb of chromosome 6 (50,500,000–52,500,000 bp). The green arrow indicates interactions of *Hoxa2* with the *Hoxa2*PTE-36kb region in E11.5 Md WT CNCCs. These interactions are reduced in E11.5 Md *Ezh2cKO* CNCCs and are completely lost in Md of E11.5 *Hoxa2PTE-36kb*$^{del/del}$ mutant embryos. The pink arrows highlight the gain of ectopic short-range interactions by *Hoxa2* in Md of E11.5 *Ezh2cKO* and *Hoxa2PTE-36kb*$^{del/del}$ mutant embryos. (**c**) Hi-C interaction heat-maps at 10kb resolution spanning a 2 Mb region of chromosome 6, including the *Hoxa* cluster and the HIRE1/HIRE2 super-enhancer regions of *Hoxa2* (50,500,000–52,500,000 bp), in E11.5 Md WT and *Ezh2cKO* CNCCs as well as in Md of *Hoxa2PTE-36kb*$^{del/del}$ mutant embryos. The calculated insulation scores for each CNCC subpopulation are shown below the Hi-C interaction heat-maps. Red arrows indicate the detected TAD borders in each condition, demonstrating that no changes occur at these boundaries. In (**b**) and (**c**), black arrows highlight reduced interactions in *Ezh2cKO* CNCCs, between the *Hoxa2* locus and Pc-marked regions. (**d**) Genome browser view of chromosome 6 (51,160,048–51,215,000) showing ChIP-seq profiles of H3K27me3 (red), H3K4me2 (green) and H3K27ac (blue) in E8.5 WT pre-migratory progenitors and E11.5 WT Md and second pharyngeal arch (PA2) CNCCs. CTCF binding sites (black) in E10.5 WT Md and PA2 are also shown. Genomic coordinates of the deleted elements are indicated by yellow boxes at the top. The PA2 tracks are shown in Fig. 7 as well.


a
Hoxa2 expression
WT vs. CTCF1+2del/del
E10.5
b
Hoxa2 expression
WT vs. RE5.5del/del
E10.5
c
Hoxa2 expression
WT vs. CTCF3+4del/del
E10.5
2-ΔΔCt
1.5
1.0
0.5
0.0
ns
PA2 WT
PA2 CTCF1+2del/del
PA2 RE5.5del/del
PA2 CTCF3+4del/del
Md WT
Md CTCF3+4del/del
Hoxa2EGFPwt
CTCF1+2del/wt ; Hoxa2EGFPwt
RE5.5del/wt ; Hoxa2EGFPwt
CTCF3+4del/wt ; Hoxa2EGFPwt
d
e
f
g
h
i
j
k
l
m
n
o
osq
sq
i
m
s
st
g
mc
t
lh
h
gh
sh
th
lp
tr

Supplementary Figure 23: Effect of RE5.5, CTCF1+2 and CTCF3+4 deletions on *Hoxa2* expression and PA2-derived skeletal structures patterning

(**a-c**) Relative expression levels of *Hoxa2*, measured by qRT-PCR, in E10.5 second pharyngeal arch (PA2) from WT and *CTCF1+2*$^{del/del}$ mutant embryos (**a**), in E10.5 PA2 from WT and *RE5.5*$^{del/del}$ mutant embryos (**b**) and in E10.5 mandibular process (Md) and PA2 from WT and *CTCF3+4*$^{del/del}$ mutant embryos (**c**). n=3 biological replicates per genotype; data are presented as mean values +/- SD. P-value: Welch's t-test (two-sided). (**d-o**) Middle ear (**d**, **e**, **g**, **h**, **j**, **k**, **m**, **n**) and hyoid (**f**, **i**, **l**, **o**) skeletal preparations from E18.5 fetuses: *Hoxa2*$^{EGFP/wt}$ (control) (**d-f,** also shown in Fig. 7), *CTCF1+2*$^{del/wt}$;*Hoxa2*$^{EGFP/wt}$ trans-heterozygous mutant (**g-i**), *RE5.5*$^{del/wt}$;*Hoxa2*$^{EGFP/wt}$ trans-heterozygous mutant (**j-l**) and *CTCF3+4*$^{del/wt}$;*Hoxa2*$^{EGFP/wt}$ trans-heterozygous mutant (**m-o**). *CTCF1+2*$^{del/wt}$;*Hoxa2*$^{EGFP/wt}$, *RE5.5*$^{del/wt}$;*Hoxa2*$^{EGFP/wt}$ and *CTCF3+4*$^{del/wt}$;*Hoxa2*$^{EGFP/wt}$ mutant fetuses display a cartilage nodule on the styloid process (st) (black arrows in **g**, **j**, and **m)** compared to controls (**d**). (**g-o**) are representative images of *CTCF1+2*$^{del/wt}$;*Hoxa2*$^{EGFP/wt}$ (n=7/8) (**g-i**), *RE5.5*$^{del/wt}$;*Hoxa2*$^{EGFP/wt}$ (n=9/10) (**j-l**) and *CTCF3+4*$^{del/wt}$;*Hoxa2*$^{EGFP/wt}$ (n=3/8) (**m-o**) fetus sides. *CTCF1+2*$^{del/wt}$;*Hoxa2*$^{EGFP/wt}$ mutant can also display a gap within the styloid process (white arrow in **g**). i, incus; g, gonial bone; gh, greater horn of the hyoid bone; lh, lesser horn of the hyoid bone; lp, lateral process of laryngeal cartilage; m, malleus; mc, Meckel cartilage; osq, retrotympanic process of squamosal bone; s, stapes; sh, superior horns of thyroid cartilage; sq, squamosal bone; t, tympanic bone; th, thyroid cartilage; tr trachea. Scale bars represent 500 µm.